

Local convergence of min-max algorithms to differentiable equilibrium on Riemannian manifold

Sixin Zhang

Université de Toulouse, INP, IRIT
2, rue Camichel, BP 7122, 31071 Toulouse Cedex 7, France
sixin.zhang@irit.fr

Abstract

We study min-max algorithms to solve zero-sum differentiable games on Riemannian manifold. The notions of differentiable Stackelberg equilibrium and differentiable Nash equilibrium in Euclidean space are generalized to Riemannian manifold, through an intrinsic definition which does not depend on the choice of local coordinate chart of manifold. We then provide sufficient conditions for the local convergence of the deterministic simultaneous algorithms τ -GDA and τ -SGA near such equilibrium, using a general methodology based on spectral analysis. These algorithms are extended with stochastic gradients and applied to the training of Wasserstein GAN. The discriminator of GAN is constructed from Lipschitz-continuous functions based on Stiefel manifold. We show numerically how the insights obtained from the local convergence analysis may lead to an improvement of GAN models.

1 Introduction

Riemannian min-max problem has attracted a lot of research attention in recent years, with various machine learning applications including robust PCA [22], robust neural network training [20] and generative adversarial networks (GANs) [17]. This problem is formalized as a two-player zero-sum game, where the variables of each player are constrained on the Riemannian manifold \mathcal{M}_1 and \mathcal{M}_2 ,

$$\min_{x \in \mathcal{M}_1} \max_{y \in \mathcal{M}_2} f(x, y).$$

When \mathcal{M}_1 and \mathcal{M}_2 are Euclidean, gradient-based methods such as gradient-descent-ascent (GDA) [10, 25], extra-gradient [15, 27], optimistic mirror descent [29], Hamiltonian-gradient descent [26] and symplectic gradient-adjustment (SGA) [4] are often considered to solve this problem. When \mathcal{M}_1 and \mathcal{M}_2 are Riemannian, how to extend existing algorithms from Euclidean space to Riemannian manifold and how to analyze their convergence become an interesting topic in recent years. In Table 1, we summarize several related works on the Riemannian min-max problem. In particular, we observe that under suitable assumptions of the problem, one can obtain the global convergence of a suitable algorithm towards certain limit set such as Nash equilibrium. One major issue is that these assumptions typically do not hold in applications such as GANs [33]. However, when a min-max problem is non-convex and non-concave, even in the Euclidean case, the limit set of GDA algorithm can be very complicated [18]. As a consequence, we aim to develop suitable concepts of limit set and algorithms with local convergence guarantees for an interesting class of problems [21].

In this article, we study the convergence of simultaneous min-max algorithms in order to find differentiable Stackelberg equilibrium (DSE) or differentiable Nash equilibrium (DNE). When \mathcal{M}_1 and \mathcal{M}_2 are Euclidean, these two limit sets are generic among local Stackelberg or Nash equilibrium of smooth f [13]. The main contribution of this article is to generalize these concepts to the Riemannian min-max problem, and to analyze the local convergence of two representative

Table 1: Related works of Riemannian min-max problem

Ref.	Class of problem	Limit set	Algorithm
[41]	Geodesically convex $\mathcal{M}_1, \mathcal{M}_2$ f is geodesically convex/concave (quasi), semi-continuous (lower/upper)	Nash equilibrium	Extra-gradient
[22]	+Bounded $\mathcal{M}_1, \mathcal{M}_2$ f is geodesically convex/concave, smooth	Nash equilibrium	Extra-gradient
[17]	Complete $\mathcal{M}_1, \mathcal{M}_2$ $(x, y) \mapsto \ \text{grad}_x f\ _x^2 + \ \text{grad}_y f\ _y^2$ is Polyak-Łojasiewicz	Stationary point of f	Hamiltonian (consensus)
[20]	Euclidean \mathcal{M}_2 f is strongly concave in y	Stationary point of $\max_y f$	GDA (accelerated)
This work	f is twice continuously differentiable	Differentiable equilibrium	GDA, SGA

deterministic min-max algorithms to such equilibrium. We further develop these algorithms using stochastic-gradients and analyze numerically their behavior in the training of Wasserstein GANs.

Section 2 provides the definition of DSE and DNE when \mathcal{M}_1 and \mathcal{M}_2 are finite-dimensional Riemannian manifolds. By using a local coordinate chart near such equilibrium, we generalize these concepts in Euclidean space [13, 38], and show that their definitions only rely on intrinsic quantities of the manifolds. Using the same local coordinate chart, we then provide a methodology to analyze the local convergence of deterministic simultaneous algorithms to a stationary point in Section 3.1. It is based on the classical Ostrowski Theorem to analyze the stability of a fixed point in one-step stationary methods [31]. This methodology is general in the sense that the problem is reduced to the spectral analysis of a Jacobian matrix in Euclidean space, which is at the heart of analyzing various min-max algorithms [10, 3, 12, 40, 24, 11]. We focus on two algorithms τ -GDA and τ -SGA, where the variables (x, y) are updated simultaneously at each iteration with a learning rate ratio τ . In Section 3.2, sufficient conditions on τ are given to ensure the local convergence of τ -GDA to DSE and DNE. One issue of τ -GDA is its slow convergence rate when there is strong rotational dynamics [24]. This is a known phenomenon near a Nash equilibrium in bilinear games due to the competition between the two players [4]. To improve the convergence rate, first-order methods such as extra-gradient and optimistic mirror descent are often used to correct the gradient direction of τ -GDA. Recently, these methods are extended to Riemannian manifold [41, 19, 37]. However, their computations rely on the exponential map and parallel transport which can be costly [1]. In Section 3.3, we consider the τ -SGA algorithm which addresses the same rotational problem based on auto-differentiation. It naturally extends the SGA algorithm [14, 4, 23] to Riemannian manifold. We further provide an asymptotic convergence analysis of τ -SGA to DSE which is valid when τ is large. In Section 4, we apply stochastic τ -GDA and τ -SGA to train Wasserstein GAN. The underlying min-max problem is Riemannian since we impose Stiefel manifold constraints on y to construct Lipschitz-continuous discriminators. We consider two examples, where one of the discriminators is build upon the wavelet scattering transform to capture discriminative information in MNIST dataset [8]. We illustrate a local convergence dilemma faced by τ -GDA, and show how τ -SGA may lead to an improved local convergence and generator quality of GAN compared to τ -GDA. Section 5 concludes.

2 Differentiable equilibrium on Riemannian manifold

In this article, we assume that $f : \mathcal{M}_1 \times \mathcal{M}_2 \rightarrow \mathbb{R}$ is twice continuously differentiable on the product manifold $\mathcal{M}_1 \times \mathcal{M}_2$. The dimension of \mathcal{M}_1 is d_1 , and the dimension of \mathcal{M}_2 is d_2 . This section introduces the notions of differentiable Stackelberg differentiable and differentiable Nash equilibrium, and gives some simple examples to illustrate their difference.

2.1 Differentiable Stackelberg equilibrium (DSE)

To define the notion of DSE on Riemannian manifold, we first introduce the definition of DSE in a local coordinate chart of $\mathcal{M}_1 \times \mathcal{M}_2$. We then show that it is equivalent to an intrinsic definition which does not depend on the choice of the coordinate chart.

Local definition of DSE Let $(O_1 \times O_2, \varphi_1 \times \varphi_2)$ be a local coordinate chart around $(x^*, y^*) \in \mathcal{M}_1 \times \mathcal{M}_2$. We rewrite the function $f(x, y)$ on $(x, y) \in O_1 \times O_2$ using this chart by

$$\bar{f}(u_1, u_2) = f(\varphi_1^{-1}(u_1), \varphi_2^{-1}(u_2)).$$

The next definition of DSE based on \bar{f} is consistent with the standard definition of DSE in Euclidean space [13, 38]. Let ∂ and ∂^2 denote the first-order and second-order partial derivatives of a function on Euclidean space.

Definition 2.1. We say that (x^*, y^*) is a DSE of f if $(u_1^*, u_2^*) = (\varphi_1(x^*), \varphi_2(y^*))$ is a DSE of \bar{f} , i.e.

$$\partial_{u_1} \bar{f}(u_1^*, u_2^*) = 0, \quad \partial_{u_2} \bar{f}(u_1^*, u_2^*) = 0, \quad (1)$$

$$- \partial_{u_2 u_2}^2 \bar{f}(u_1^*, u_2^*) \quad p.d. \text{ (abbrev. of positive definite)}, \quad (2)$$

$$[\partial_{u_1 u_1}^2 \bar{f} - \partial_{u_2 u_1}^2 \bar{f} \cdot (\partial_{u_2 u_2}^2 \bar{f})^{-1} \cdot \partial_{u_1 u_2}^2 \bar{f}](u_1^*, u_2^*) \quad p.d. \quad (3)$$

The condition (1) alone means that (u_1^*, u_2^*) is a stationary point of \bar{f} . The conditions (1),(2),(3) imply that (u_1^*, u_2^*) is a local minimax point of \bar{f} [21, 38]. See further discussions in Appendix A.

Intrinsic definition of DSE We denote the tangent space of \mathcal{M}_1 at $x \in \mathcal{M}_1$ by $T_x \mathcal{M}_1$ and the tangent space of \mathcal{M}_2 at $y \in \mathcal{M}_2$ by $T_y \mathcal{M}_2$. The following concepts are standard in manifold optimization, and they are used in Riemannian min-max problem [17].

- Riemannian gradient: $\text{grad}_x f(x, y) \in T_x \mathcal{M}_1, \text{grad}_y f(x, y) \in T_y \mathcal{M}_2$.
- Riemannian Hessian: $\text{Hess}_x f(x, y) : T_x \mathcal{M}_1 \rightarrow T_x \mathcal{M}_1, \text{Hess}_y f(x, y) : T_y \mathcal{M}_2 \rightarrow T_y \mathcal{M}_2$.
- Riemannian cross-gradient: $\text{grad}_{xy}^2 f(x, y) : T_x \mathcal{M}_1 \rightarrow T_y \mathcal{M}_2, \text{grad}_{yx}^2 f(x, y) : T_y \mathcal{M}_2 \rightarrow T_x \mathcal{M}_1$.

Definition 2.2. We say that (x^*, y^*) is a DSE of f if

$$\text{grad}_x f(x^*, y^*) = 0, \quad \text{grad}_y f(x^*, y^*) = 0, \quad (4)$$

$$- \text{Hess}_y f(x^*, y^*) \quad p.d., \quad (5)$$

$$[\text{Hess}_x f - \text{grad}_{yx}^2 f \cdot (\text{Hess}_y f)^{-1} \cdot \text{grad}_{xy}^2 f](x^*, y^*) \quad p.d. \quad (6)$$

The following result shows that the above two definitions are equivalent, no matter how one choose the local coordinate chart nearby (x^*, y^*) , or the Riemannian metric on $\mathcal{M}_1 \times \mathcal{M}_2$.

Theorem 2.1. The local definition of DSE in Definition 2.1 is equivalent to the intrinsic definition of DSE in Definition 2.2.

The proof is given in Appendix B. The main idea of the proof is to use the local coordinate chart $(O_1 \times O_2, \varphi_1 \times \varphi_2)$ to represent the smooth vector fields $(x, y) \mapsto \text{grad}_x(x, y)$ and $(x, y) \mapsto \text{grad}_y(x, y)$ around the point (x^*, y^*) , so as to show the equivalence between (1)-(3) and (4)-(6).

2.2 Differentiable Nash equilibrium (DNE) and examples

In game theory, one is often interested in finding a Nash equilibrium since it maintains a symmetry between the role of the two players. Based on the intrinsic definition of DSE, we immediately obtain an intrinsic definition of DNE. We then provide some simple examples of DSE and DNE.

Definition 2.3. We say that (x^*, y^*) is a DNE of f if

$$\text{grad}_x f(x^*, y^*) = 0, \quad \text{grad}_y f(x^*, y^*) = 0, \quad (7)$$

$$- \text{Hess}_y f(x^*, y^*) \quad p.d., \quad \text{Hess}_x f(x^*, y^*) \quad p.d. \quad (8)$$

The definition of DNE generalizes an equivalent notion “strongly local min-max point” in Euclidean space [10, Definition 1.6]. It is clear that if (x^*, y^*) is a DNE, then it is also a DSE.

2.2.1 Example 1: DSE

Consider $f(x, y) = \langle y, Ax - b \rangle$, with $x \in \mathcal{M}_1 = \mathbb{R}^{d_1}$ and $y \in \mathcal{M}_2 = S^{d_2}$. The manifold S^{d_2} is the unit sphere embedded in \mathbb{R}^{d_2+1} , endowed with the Euclidean metric $\langle \cdot, \cdot \rangle$ on \mathbb{R}^{d_2+1} . Let A^+ denote the pseudo-inverse of A . We next provide a sufficient condition on the existence of DSE.

Proposition 2.1. Assume $b \notin \text{Range}(A)$, $\text{Ker}(A) = \{0\}$. Let $x^* = A^+b$, $y^* = \frac{Ax^* - b}{\|Ax^* - b\|}$, then (x^*, y^*) is a DSE of the f in Example 1.

The proof is given in Appendix C. Since \mathcal{M}_1 is Euclidean, we note that $\partial_{xx}^2 f(x^*, y^*) = 0$. This implies that the (x^*, y^*) is not DNE. But the k -th eigenvalue $\lambda_k(\mathbf{A})$ of $\mathbf{A} = -\text{Hess}_y f(x^*, y^*)$ equals to $\|Ax^* - b\| > 0$, since from the proof $\langle \mathbf{A}[\eta^*], \eta^* \rangle = \|Ax^* - b\| \|\eta^*\|^2$ for any $\eta^* \in T_{y^*} \mathcal{M}_2$.

2.2.2 Example 2: DSE

Consider $f(x, y) = \langle y, Ax - b \rangle - \frac{\kappa}{2} \|Ax\|^2$, with $x \in \mathcal{M}_1 = \mathbb{R}^{d_1}$ and $y \in \mathcal{M}_2 = S^{d_2}$. Compared to the f in Example 1, we add a quadratic function of Ax with a curvature parameter $\kappa > 0$. We next show that if κ is close to zero, we can still find a DSE near the DSE in Proposition 2.1.

Proposition 2.2. Assume $b \notin \text{Range}(A)$, $\text{Ker}(A) = \{0\}$. There exists $\kappa_0 > 0$ such that for any $0 < \kappa < \kappa_0$, there is a number c close to 1, and $x^* = cA^+b$, $y^* = \frac{Ax^* - b}{\|Ax^* - b\|}$, so that (x^*, y^*) is a DSE of the f in Example 2.

The proof is given in Appendix D. From the proof, we have $\mathbf{C} = \partial_{xx}^2 f(x, y) = -\kappa A^\top A$. The spectral radius of \mathbf{C} equals to its operator norm $\|\mathbf{C}\| = \kappa \|A^\top A\| > 0$. As Example 1, all the eigenvalues of $\mathbf{A} = -\text{Hess}_y f(x^*, y^*)$ equal to $\|Ax^* - b\| = \|cAA^+b - b\|$. These quantities will be used later to analyze the local convergence of τ -GDA and τ -SGA.

2.2.3 Example 3: DNE

Consider $f(x, y) = \frac{1}{2} \|Ax + y - b\|^2$ with $x \in \mathcal{M}_1 = \mathbb{R}^{d_1}$ and $y \in \mathcal{M}_2 = S^{d_2}$. \mathcal{M}_2 is the same embedded sub-manifold of \mathbb{R}^{d_2+1} as above. We next provide a sufficient condition on the existence of DNE. The proof is given in Appendix E.

Proposition 2.3. Assume $b \notin \text{Range}(A)$, $\text{Ker}(A) = \{0\}$. Let $x^* = A^+b$, $y^* = \frac{Ax^* - b}{\|Ax^* - b\|}$, then (x^*, y^*) is a DNE of the f in Example 3.

3 Min-max algorithms for differentiable equilibrium

Gradient-based min-max algorithms such as GDA and SGA are often used to find local Nash equilibrium when \mathcal{M}_1 and \mathcal{M}_2 are Euclidean [10, 23]. We study how to extend these algorithms to Riemannian manifold and then analyze their local convergence to DSE and DNE.

3.1 Local convergence of deterministic simultaneous algorithms

We analyze the local convergence of one-step deterministic algorithms to a stationary point. As the update rule of each algorithm in this family does not change over iteration, we represent it in a local coordinate chart and then apply the proof technique of the classical Ostrowski Theorem.

A deterministic simultaneous algorithm is defined by two vector fields $(x, y) \mapsto \xi_1(x, y)$, $(x, y) \mapsto \xi_2(x, y)$ on \mathcal{M}_1 and \mathcal{M}_2 , and a choice of manifold retractions. Initialized at a point on $\mathcal{M}_1 \times \mathcal{M}_2$, the algorithm modifies the variables (x, y) of the two players, through an update rule $\mathbf{T} : \mathcal{M}_1 \times \mathcal{M}_2 \rightarrow \mathcal{M}_1 \times \mathcal{M}_2$ of the following form,

$$\mathbf{T}(x, y) = (\mathcal{R}_{1,x}(\xi_1(x, y)), \mathcal{R}_{2,y}(\xi_2(x, y))),$$

where $\mathcal{R}_{1,x} : T_x \mathcal{M}_1 \rightarrow \mathcal{M}_1$ (resp. $\mathcal{R}_{2,y} : T_y \mathcal{M}_2 \rightarrow \mathcal{M}_2$) denotes the restriction of a retraction \mathcal{R}_1 at $x \in \mathcal{M}_1$ (resp. retraction of \mathcal{R}_2 at $y \in \mathcal{M}_2$). For example, on the $\mathcal{M}_1 = \mathbb{R}^{d_1}$ and $\mathcal{M}_2 = S^{d_2}$ in Section 2.2, we will take $\mathcal{R}_{1,x}(\delta) = x + \delta$ for $\delta \in \mathbb{R}^{d_1}$, and $\mathcal{R}_{2,y}(\eta)$ to be the projection of the vector $y + \eta$ in \mathbb{R}^{d_2+1} to the sphere \mathcal{M}_2 .

We next define what it means for an update rule \mathbf{T} to be locally convergent to a stationary point (x^*, y^*) , which implies that (x^*, y^*) is a point of attraction [31, Definition 10.1.1].

Definition 3.1 (locally convergent). Let (x^*, y^*) be a stationary point satisfying (4). There exists a local stable region $S_\delta \subset \mathcal{M}_1 \times \mathcal{M}_2$, which is an open set containing (x^*, y^*) such that started from $(x(0), y(0)) \in S_\delta$, the update rule generates a sequence of points $(x(t+1), y(t+1)) = \mathbf{T}(x(t), y(t))$ belonging to S_δ , $\forall t \geq 0$, and moreover $\lim_{t \rightarrow \infty} (x(t), y(t)) = (x^*, y^*)$.

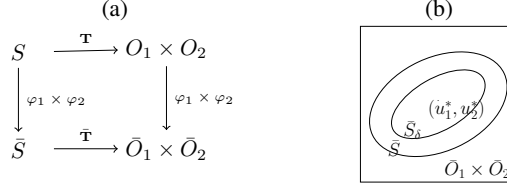


Figure 1: Local convergence of a deterministic simultaneous algorithm. (a): The update rule \mathbf{T} on the manifold $\mathcal{M}_1 \times \mathcal{M}_2$ induces a local update rule $\bar{\mathbf{T}}$ in the local coordinate system, defined by a chart $(O_1 \times O_2, \varphi_1 \times \varphi_2)$ around (x^*, y^*) . (b): The induced update rule $\bar{\mathbf{T}}$ is defined in the local coordinate on the set \bar{S} around $(u_1^*, u_2^*) = \varphi_1 \times \varphi_2 \circ (x^*, y^*)$. It contains a stable region \bar{S}_δ .

We next give a sufficient condition for \mathbf{T} to be locally convergent to (x^*, y^*) . It is based on the spectral radius of the following linear transformation on $T_{x^*}\mathcal{M}_1 \times T_{y^*}\mathcal{M}_2$,

$$\mathbf{T}'(x^*, y^*) = \begin{pmatrix} I + \nabla_x \xi_1(x^*, y^*) & D_y \xi_1(x^*, y^*) \\ D_x \xi_2(x^*, y^*) & I + \nabla_y \xi_2(x^*, y^*) \end{pmatrix}, \quad (9)$$

where D_x and ∇_x (resp. D_y and ∇_y) denote the differential operator (in a tangent map) and the Riemannian connection on \mathcal{M}_1 (resp. on \mathcal{M}_2).

Theorem 3.1. *Let $(x^*, y^*) \in \mathcal{M}_1 \times \mathcal{M}_2$ be a stationary point of f . If ξ_1 and ξ_2 are differentiable on $\mathcal{M}_1 \times \mathcal{M}_2$, and the spectral radius of $\mathbf{T}'(x^*, y^*)$ is strictly smaller than one, then \mathbf{T} is locally convergent to (x^*, y^*) .*

Proof. The idea of the proof is illustrated in Figure 1. Inspired by the proof technique in [7, Theorem 4.19], we first identify a set \bar{S} so that the induced dynamics $\bar{\mathbf{T}}$ is well-defined on \bar{S} . Let us consider the set $S = \mathbf{T}^{-1}(O_1 \times O_2) \cap (O_1 \times O_2)$ and its local coordinate domain $\bar{S} = (\varphi_1 \times \varphi_2)(S) \subset \bar{O}_1 \times \bar{O}_2$. We can therefore write both $(x, y) \in S \subset O_1 \times O_2$ and $\mathbf{T}(x, y) \in O_1 \times O_2$ in local coordinate, i.e. $\forall (u_1, u_2) \in \bar{S}$,

$$\bar{\mathbf{T}}(u_1, u_2) = \varphi_1 \times \varphi_2 \circ (\mathbf{T}(\varphi_1^{-1}(u_1), \varphi_2^{-1}(u_2))).$$

Note that S and \bar{S} are non-empty open sets since \mathbf{T} is continuous (by the continuity of the vector fields ξ_1, ξ_2 and the retractions \mathcal{R}_1 and \mathcal{R}_2) and (x^*, y^*) is a fixed point of \mathbf{T} . We next identify a local stable region $\bar{S}_\delta \subset \bar{S}$ around (u_1^*, u_2^*) (the local coordinate of (x^*, y^*)), so that if $(u_1, u_2) \in \bar{S}_\delta$, then $\bar{\mathbf{T}}(u_1, u_2) \in \bar{S}_\delta \subset \bar{O}_1 \times \bar{O}_2$. Let $\bar{S}_\delta = (\varphi_1 \times \varphi_2)^{-1} \circ (\bar{S}_\delta)$, and assume $(x(0), y(0)) \in \bar{S}_\delta$, then the sequence $(x(t), y(t)) \in \bar{S}_\delta \subset S, \forall t \geq 1$ by recursion. To construct such a region, the key is to verify that the spectral radius ρ of the Jacobian matrix $\bar{\mathbf{T}}'(u_1^*, u_2^*)$ is strictly smaller than one (in Appendix F, we show that the eigenvalues of $\mathbf{T}'(x^*, y^*)$ are the same as $\bar{\mathbf{T}}'(u_1^*, u_2^*)$), so that according to the proof of Ostrowski Theorem in [31, Section 10.1.3], for an arbitrary $\epsilon > 0$, there exists a norm $\|\cdot\|_\epsilon$ on $\mathbb{R}^{d_1} \times \mathbb{R}^{d_2}$ and $\delta > 0$, satisfying

$$\|\bar{\mathbf{T}}(u_1, u_2) - (u_1^*, u_2^*)\|_\epsilon \leq (\rho + 2\epsilon)\|(u_1, u_2) - (u_1^*, u_2^*)\|_\epsilon, \quad \forall (u_1, u_2) \in \bar{S}_\delta, \quad (10)$$

where $\bar{S}_\delta = \{(u_1, u_2) \mid \|(u_1, u_2) - (u_1^*, u_2^*)\|_\epsilon < \delta\} \subset \bar{S}$. Let's choose ϵ so that $\rho + 2\epsilon < 1$, then from (10), if $(u_1(0), u_2(0)) \in \bar{S}_\delta$, the sequence $(u_1(t), u_2(t))$ stays in \bar{S}_δ and converges to (u_1^*, u_2^*) as $t \rightarrow \infty$. As $\varphi_1 \times \varphi_2$ is a continuous bijection (homeomorphism) from $O_1 \times O_2$ to $\bar{O}_1 \times \bar{O}_2$, we have equivalently that if $(x(0), y(0)) \in \bar{S}_\delta = (\varphi_1 \times \varphi_2)^{-1} \circ (\bar{S}_\delta)$, the sequence $(x(t), y(t))$ will stay in \bar{S}_δ and converges to (x^*, y^*) . \square

3.2 Simultaneous gradient-descent-ascent algorithm (τ -GDA)

The τ -GDA algorithm uses the Riemannian gradients $\text{grad}_x f(x, y)$ and $\text{grad}_y f(x, y)$ to update x and y simultaneously. The local convergence of deterministic τ -GDA to DSE and DNE is known in Euclidean space [10, 12, 21, 24]. This section extends these results to Riemannian manifold. We obtain a sharp lower-bound of τ for τ -GDA to be locally convergent to DSE, based on a refinement of the spectral analysis in Euclidean space [24].

τ -GDA algorithm In deterministic setting, the update rule \mathbf{T} of τ -GDA is determined by

$$\xi_1(x, y) = -\gamma \text{grad}_x f(x, y), \quad \xi_2(x, y) = \tau \gamma \text{grad}_y f(x, y). \quad (11)$$

Note that $\gamma > 0$ and we use a ratio $\tau > 0$ to adjust the learning rate (step size) of the Riemannian gradients. The deterministic τ -GDA can be readily extended to stochastic τ -GDA by using an unbiased estimation of the Riemannian gradients [22, 20].

Local convergence of deterministic τ -GDA Based on Theorem 3.1, we obtain the following local convergence of τ -GDA to DSE on Riemannian manifold. We rewrite the Riemannian Hessian and cross-gradient in the following linear transform on $T_{x^*} \mathcal{M}_1 \times T_{y^*} \mathcal{M}_2$ using $(\mathbf{A}, \mathbf{B}, \mathbf{C})$, i.e.

$$\begin{pmatrix} -\mathbf{C} & -\mathbf{B} \\ \tau \mathbf{B}^\top & -\tau \mathbf{A} \end{pmatrix} = \begin{pmatrix} -\text{Hess}_x(x^*, y^*) & -\text{grad}_{yx}^2 f(x^*, y^*) \\ \tau \text{grad}_{xy}^2 f(x^*, y^*) & \tau \text{Hess}_y(x^*, y^*) \end{pmatrix}. \quad (12)$$

Theorem 3.2. Assume (x^*, y^*) is a DSE of f . If $\tau > \frac{\max_k |\lambda_k(\mathbf{C})|}{\lambda_{\min}(\mathbf{A})}$, then there exists $\gamma^\bullet > 0$ such that for any $0 < \gamma < \gamma^\bullet$, the τ -GDA (defined by (11)) is locally convergent to (x^*, y^*) .

The proof is given Appendix G. When \mathcal{M}_1 and \mathcal{M}_2 are Euclidean, the range $\{\tau \in \mathbb{R}_+ | \tau > \|\partial_{xx}^2 f(x^*, y^*)\| / \lambda_{\min}(-\partial_{yy}^2 f(x^*, y^*))\}$ in Theorem 3.2 is broader compared to the range given in [24, Theorem 4.2]. Moreover, this range is sharp as one can construct a counter-example [24, Theorem 4.1] to show that if τ is outside this range, the spectral radius of the Jacobian matrix (9) is strictly larger than one for any $\gamma > 0$.

We next analyze the local convergence of τ -GDA to DNE. Theorem 3.2 can be readily applied. However, we can obtain a broader range of τ . In Euclidean space, the local convergence to DNE is analyzed in [10, Theorem 1.10] when $\tau = 1$, and generalized to $\tau > 0$ in [21, Proposition 26].

Theorem 3.3. Assume (x^*, y^*) is a DNE of f . If $\tau > 0$, then there exists $\gamma^\bullet > 0$ such that for any $0 < \gamma < \gamma^\bullet$, the τ -GDA (defined by (11)) is locally convergent to (x^*, y^*) .

The proof is given in Appendix H. Different to the proof of Theorem 3.2, we analyze the spectral radius of the Jacobian matrix (9) based on the Ky Fan inequality [39, Lemma 4.20] as in [10].

3.3 Symplectic gradient-adjustment method (τ -SGA)

In Euclidean space, SGA modifies a vector field ξ in an update rule $\mathbf{T}(x, y) = (x, y) + \gamma \xi(x, y)$ so that it allows one to cross the curl of ξ which would otherwise results in a strong rotational dynamics near a stationary point [14]. We apply this idea to τ -GDA on Riemannian manifold and analyze its local convergence to DSE when τ is large.

τ -SGA algorithm SGA adjusts the vector field ξ using an orthogonal vector field which is constructed from the anti-symmetric part of the Jacobian matrix of ξ . In τ -GDA, $\xi(x, y) = (-\delta(x, y), \tau \eta(x, y))$ where $\delta(x, y) = \text{grad}_x f(x, y)$ and $\eta(x, y) = \text{grad}_y f(x, y)$. The adjustment of τ -SGA is based on the Riemannian cross-gradients $\tilde{\mathbf{B}}(x, y) = \text{grad}_{yx}^2 f(x, y)$ and $\tilde{\mathbf{B}}^\top(x, y) = \text{grad}_{xy}^2 f(x, y)$, which results in the following vector fields in the update rule,

$$\xi_1(x, y) = -\gamma \left(\delta(x, y) + \mu \frac{(\tau + 1)\tau}{2} \tilde{\mathbf{B}}(x, y)[\eta(x, y)] \right), \quad (13)$$

$$\xi_2(x, y) = \gamma \left(\tau \eta(x, y) - \mu \frac{\tau + 1}{2} \tilde{\mathbf{B}}^\top(x, y)[\delta(x, y)] \right), \quad (14)$$

where $\mu \in \mathbb{R}$ is a hyper-parameter. In Appendix I, we detail the derivation of the update rule, and verify that the adjusted direction $(-\tau \tilde{\mathbf{B}}[\eta], -\tilde{\mathbf{B}}^\top[\delta])$ is orthogonal to $\xi = (-\delta, \tau \eta)$ at each point (x, y) . In Appendix J, we discuss how to perform (stochastic) gradient adjustment using auto-differentiation when \mathcal{M}_1 and \mathcal{M}_2 are Euclidean embedded sub-manifolds [1, Chapter 3.3].

Local convergence of deterministic τ -SGA: asymptotic analysis We study the local convergence of the deterministic τ -SGA to DSE in an asymptotic regime where $\tau \rightarrow \infty$. This simplifies the update rule of τ -SGA in order to adapt the proof of Theorem 3.2. In this regime, to make the term

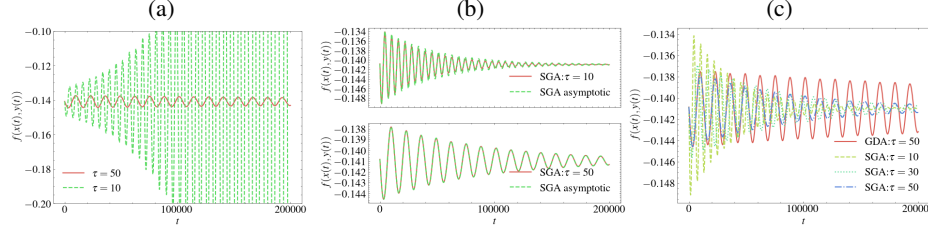


Figure 2: Evolution of $f(x(t), y(t))$ as a function of iteration t in deterministic τ -GDA and τ -SGA on Example 2 ($\gamma = 0.001/\tau, \theta = 0.15$). a). τ -GDA with $\tau = 10$ vs. $\tau = 50$. b). τ -SGA vs. asymptotic τ -SGA with $\tau = 10$ and $\tau = 50$. c). τ -GDA at $\tau = 50$ vs. τ -SGA at $\tau \in \{10, 30, 50\}$.

$\tilde{\mathbf{B}}[\eta]$ comparable to the term δ in (13), we set $\mu \sim \frac{1}{\tau^2}$. As a consequence, $\mu \frac{\tau+1}{2} \sim \frac{1}{\tau}$ and the update rule in (14) can be simplified to the ξ_2 in (11). The next theorem makes sense for τ -SGA when τ is chosen sufficiently large.

Theorem 3.4. Assume (x^*, y^*) is a DSE of f . If $\tau > \min \left(\frac{\max_k |\lambda_k(\mathbf{C})|}{\lambda_{\min}(\mathbf{A})}, \frac{\max_k |\lambda_k(\mathbf{C} + \theta \mathbf{B} \mathbf{B}^\top)|}{\lambda_{\min}(\mathbf{A})} \right)$, and $\mu = \theta \frac{2}{\tau(\tau+1)}$ with $0 \leq \theta \leq \frac{1}{\lambda_{\max}(\mathbf{A})}$, then there exists $\gamma^* > 0$ such that for any $0 < \gamma < \gamma^*$, the asymptotic τ -SGA (ξ_1 defined by (13), ξ_2 defined by (11)) is locally convergent to (x^*, y^*) .

The proof is given in Appendix K. Contrary to Theorem 3.2, the valid range of τ depends also on the choice of θ . If the spectral radius of \mathbf{C} is larger than that of $\mathbf{C} + \theta \mathbf{B} \mathbf{B}^\top$ with a suitable choice of θ , then a broader range of τ could be used in τ -SGA compared to τ -GDA. In Figure 2, we compare the local convergence rate of τ -GDA and τ -SGA in the Example 2 of Section 2.2, where $\mathbf{A} = [1; 1; 1] \in \mathbb{R}^{3 \times 1}$, $\mathbf{b} = [1; 1; 0.99] \in \mathbb{R}^3$ and $\kappa = 0.1$. In this case, we find numerically that $x^* \approx 0.9975$. The initial point of each algorithm is $x = \mathbf{A}^+ \mathbf{b}, y = (\mathbf{A}x - \mathbf{b})/\|\mathbf{A}x - \mathbf{b}\|$. In Figure 2(a), we verify the range of τ for τ -GDA convergence. According to Theorem 3.2 and the discussion after Proposition 2.2, a valid range of τ should be larger than $\frac{\max_k |\lambda_k(\mathbf{C})|}{\lambda_{\min}(\mathbf{A})} = \kappa \|\mathbf{A}^\top \mathbf{A}\|/\|\mathbf{A}x^* - \mathbf{b}\| \approx 36.18$. Figure 2(a) shows that when $\tau = 10$, τ -GDA can diverge. When $\tau = 50$, τ -GDA converges slowly to the value $\max_y f(x^*, y) = -0.141$. This is a convergence dilemma of τ -GDA: to achieve local convergence, τ needs to be large, but the rate can be very slow. In Figure 2(b) and (c), we study τ -SGA using the same learning rate $\tau\gamma$ for y . Figure 2(b) validates that the gap between the asymptotic τ -SGA and τ -SGA is not so big even if $\tau = 10$. Therefore Theorem 3.4 is valid for τ -SGA. When $\theta = 0.15$, we find that $\frac{\max_k |\lambda_k(\mathbf{C} + \theta \mathbf{B} \mathbf{B}^\top)|}{\lambda_{\min}(\mathbf{A})} \approx 16.7$, which suggests that τ -SGA can be locally convergent with a smaller τ compared to τ -GDA. Figure 2(c) confirms this analysis and it also shows that a faster rate can be achieved by τ -SGA. Surprisingly, τ -SGA quickly converges towards -0.141 even if $\tau = 10$.

The local convergence of τ -SGA to DNE in Euclidean space is analyzed in [23, Theorem 10] when $\tau = 1$. However, we could not easily extend this result to $\tau > 0$, since when $\tau \neq 1$, a DNE is not necessarily a stable fixed point of the vector field $\xi = (-\delta, \tau\eta)$, c.f [23, Definition 4]. It is thus unclear if there is a valid range of μ such that for any $\tau > 0$, τ -SGA is locally convergent to DNE.

4 Application to Wasserstein GAN

Based on the local convergence analysis of τ -GDA and τ -SGA, we apply these algorithms in the stochastic setting to train Wasserstein GAN. In the min-max problem of GAN, we assume \mathcal{M}_1 is Euclidean and \mathcal{M}_2 is Riemannian. The manifold constraint on y makes the GAN discriminator Lipschitz-continuous, so that $\max_{y \in \mathcal{M}_2} f(x, y)$ gives a lower-bound estimation of the Wasserstein-1 distance (up to multiplicative constant) between the data and the GAN generator distribution [5, 30].

4.1 Basic setup of Wasserstein GAN

In Wasserstein GAN¹, we are interested in the following min-max problem

$$f(x, y) = \mathbb{E}(D_y(\phi_{data})) - \mathbb{E}(D_y(\phi_x)),$$

¹We assume that the data is generated by the random variable $\phi_{data} \in \mathbb{R}^d$. The idea of GAN is to approximate the probability distribution of ϕ_{data} using a generator G_x parameterized by $x \in \mathcal{M}_1$. It defines a generative

where the discriminator $D_y : \mathbb{R}^d \rightarrow \mathbb{R}$ is Lipschitz-continuous. The expectations in f are taken with respect to the random variable ϕ_{data} and ϕ_x .² We consider modeling two examples of ϕ_{data} using low-dimensional generator (dimension $p < d$). More details are given in Appendix L.

Gaussian distribution by linear generator We want to model $\phi_{data} \sim \mathcal{N}(0, \Sigma)$ on $d = 5$. We focus on $p = 4$ to build a PCA-like model. The covariance matrix Σ is diagonal with a small eigenvalue, i.e. $(1, 2^2, 3^2, 4^2, 0.01)$. We choose the generator $G_x(Z) = A_x Z$, where $A_x \in \mathbb{R}^{d \times p}$ and Z is isotropic normal. For the discriminator, we denote the Stiefel manifold of k orthogonal vectors on \mathbb{R}^n by $St(k, n)$, and choose (using a smooth non-linearity ρ , c.f. Appendix L.1)

$$D_y(\phi) = \langle v_y, \rho(W_y \phi) \rangle,$$

where $W_y \in St(k, d)$, $v_y \in St(1, k)$. Since A_x is the only generator parameter, $\mathcal{M}_1 = \mathbb{R}^{d \times p}$. The discriminator parameter $y := (W_y, v_y)$, i.e. $\mathcal{M}_2 = St(k, d) \times St(1, k)$.

MNIST (digit 0) by DCGAN generator We aim to model the digit 0 in the MNIST dataset ($d = 28 \times 28$) using the DCGAN architecture ($p = 128$) in WGAN-GP [16]. The space \mathcal{M}_1 is Euclidean with dimension $d_1 = 1556673$. Unlike the CNN discriminator in WGAN-GP, we consider a hybrid Scattering CNN discriminator which has a smaller number of trainable parameters [32],

$$D_y(\phi) = \langle v_y, \rho(w_y \star P(\phi) + b_y) \rangle.$$

The scattering transform $P : \mathbb{R}^d \rightarrow \mathbb{R}^{I \times n \times n}$ is Lipschitz-continuous [8] and it has no trainable parameter. The scattering features $P(\phi) \in \mathbb{R}^{I \times n \times n}$ are computed from an image ϕ of size $\sqrt{d} \times \sqrt{d}$. We then apply an orthogonal convolutional layer to $P(\phi)$ [9]. It has the kernel orthogonality [2], by reshaping w_y (size $J \times I \times k \times k$) into a matrix $W_y \in \mathbb{R}^{J \times (Ik^2)}$ and imposing that $W_y \in St(J, Ik^2)$. The bias parameter $b_y \in \mathbb{R}^J$ and the output of the convolutional layer is reshaped into a vector in \mathbb{R}^{JN^2} . As in the Gaussian case, we further assume $v_y \in St(1, JN^2)$. In summary, $y := (W_y, b_y, v_y)$, i.e. $\mathcal{M}_2 = St(J, Ik^2) \times \mathbb{R}^J \times St(1, JN^2)$.

4.2 Results on Gaussian distribution by linear generator

To study the local convergence, we first obtain a reasonable solution (x, y) in terms of model quality (to be specified) by solving the min-max problem using τ -GDA. We then study the local convergence of τ -GDA initialized from this solution. In Figure 3(a), we show how the function value $f(x(t), y(t))$ changes over iteration. It is estimated using a batch of 1000 training samples. For each choice of $\tau \in \{1, 10, 100\}$, we set $\gamma = 0.02/\tau$. This ensures a fixed learning rate 0.02 for the discriminator. We observe that when $\tau = 1$, $f(x(t), y(t))$ has a huge oscillation, but when $\tau = 10$ and 100, it has a much smaller oscillation amplitude. To investigate the underlying reason, we compute in Figure 3(b), the evolution of an ‘‘angle’’ quantity every one thousand iterations. The angle at (x, y) is defined as $\frac{\langle v_y, \delta(x, y) \rangle}{\|\delta(x, y)\|}$, where $\delta(x, y) = \mathbb{E}(\rho(W_y \phi_{data})) - \mathbb{E}(\rho(W_y \phi_x))$ is estimated from the same batch of samples during the training. When the angle is close to 1, it indicates that v_y is solved to be optimal. We observe that when $\tau = 1$, the angle oscillates between positive and negative values, suggesting that $v_{y(t)}$ is detached from $\delta(x(t), y(t))$. Therefore the minimization of f over x does not get a good feedback to improve the model. This is confirmed in Figure 3(c), where we compute the EMD distance [34] every one thousand iterations, between the empirical measure of ϕ_{data} and $\phi_{x(t)}$ (using 2000 validation samples). We observe that the EMD distance increases over t when $\tau = 1$. On the contrary, it stays close to one when $\tau = 10$ and 100. When $\tau = 100$, we find that the covariance error $\|\Sigma - A_{x(t)} A_{x(t)}^\top\|$ stays around 0.3 over all iterations. This error is between the smallest eigenvalue of Σ (which is 0.01, the PCA error) and the second smallest eigenvalue of Σ . Therefore to use a large enough τ is crucial to avoid large model error, as it is necessary to ensure a positive angle. This phenomenon is consistent with the local convergence of τ -GDA to DSE in Figure 2(a).

model $\phi_x = G_x(Z)$, which transform a random variable $Z \in \mathbb{R}^p$ to $\phi_x \in \mathbb{R}^d$. The generator is optimized so that the distribution of ϕ_x approximates that of ϕ_{data} . This is achieved through the feedback of a discriminator function D_y , parameterized by $y \in \mathcal{M}_2$.

²In the stochastic setting, the expectation of $D_y(\phi_{data})$ (resp. $D_y(\phi_x)$) is estimated at each iteration using a batch of samples of data in the training set (resp. a batch of samples of Z). The number of samples in a batch is called batch size.

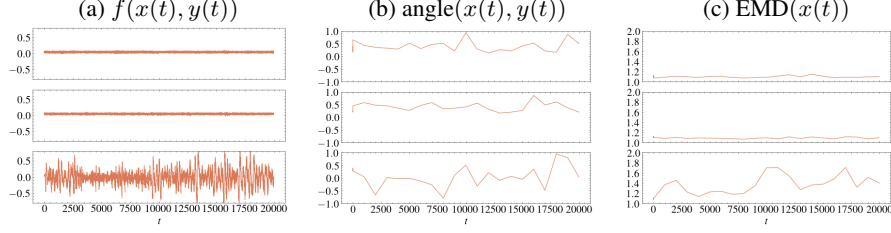


Figure 3: Evolution of $f(x(t), y(t))$, $\text{angle}(x(t), y(t))$, and $\text{EMD}(x(t))$ distance over iteration t in stochastic τ -GDA on Wasserstein GAN of Gaussian distribution. Top: $\tau = 100, \gamma = 0.0002$. Middle: $\tau = 10, \gamma = 0.002$, Bottom: $\tau = 1, \gamma = 0.02$.

Table 2: Last iteration measures in stochastic τ -GDA and τ -SGA on Wasserstein GAN of MNIST (digit 0). We report the f , angle, and FID scores computed at $(x(T), y(T))$. τ -GDA is trained for $T = 2 \times 10^5$ iterations with $\gamma = 0.05/\tau$. τ -SGA is trained longer with $\gamma = 0.01, \tau = 5, \theta = 0.075$. Only significant digits are reported with respect to the standard deviation (shown in (\pm)) of the statistical estimation of these quantities (see footnote 3 and 4).

τ -GDA					τ -SGA				
τ	f	angle	FID (train)	FID (val)	$T(10^6)$	f	angle	FID (train)	FID (val)
5	-0.09	-0.26	21	29 (± 0.9)	1	0.02	0.16	12	21 (± 0.9)
10	0.09	0.11	34	36 (± 0.6)	2	0.018	0.2	9.3 (± 0.2)	15 (± 0.5)
30	0.036	0.4	13	20 (± 0.95)	3	0.016	0.2	8.2 (± 0.2)	14 (± 0.3)

4.3 Results on MNIST (digit 0) by DCGAN generator

We study the convergence of τ -GDA and τ -SGA to improve the training of a pre-trained model obtained by alternating τ -GDA method (c.f. Appendix L.5). To measure the quality of the pre-trained model, we compute the FID scores [36]. It is estimated on both training and validation samples of MNIST.³ We obtain a pre-trained model with FID (train) 12 and FID (val) 18. The results of τ -GDA and τ -SGA using batch size 128, initialized from this pre-trained model, are reported in Table 2. For τ -GDA, we choose $\gamma = 0.05/\tau$ among $\tau \in \{5, 10, 30\}$. We observe that when $\tau = 30$, τ -GDA has a more stable dynamics than $\tau = 5$ and 10 because the angle stays around a positive constant.⁴ On the other hand, a larger τ tends to slowdown the reduction of f as shown in Figure 2(a). Due to the stochastic gradients, we observe a stagnation of f over iteration when $\tau = 30$. Indeed, the FID scores at $T = 3 \times 10^6$ are similar to those at $T = 2 \times 10^5$. Facing such a convergence dilemma, we evaluate the performance of τ -SGA using $\tau = 5$ such that $\tau\gamma$ remains the same. This is the case where τ -GDA is not convergent due to oscillating angles. We find that both the angle and the FID scores are significantly improved with a suitable choice of θ and T in τ -SGA.

5 Conclusion

In this article, we extend the notions of DSE and DNE to Riemannian manifold from Euclidean space, and then study the local convergence of τ -GDA and τ -SGA in theory. Our theoretical results are based on the spectral analysis of an intrinsic Jacobian matrix analyzed in local coordinate. This methodology can be served as a basis to analyze other algorithms. However, this local analysis approach may not be suitable to analyze stochastic algorithms since they typically have a more global behavior. For this reason, we study stochastic τ -GDA and τ -SGA numerically, where we observe certain phenomenon similar to our theoretical results, such as the importance of the choice of a suitable τ to ensure the local convergence to DSE. From this insight, we are able to improve the convergence of stochastic τ -GDA in Wasserstein GANs, leading to a better generative model.

³To compute FID (train) (resp. FID (val)), we generate the same number of fake samples as the training samples (resp. as the validation samples), and report an average value by re-sampling the fake samples 10 times.

⁴To compute the angle, we estimate $\delta(x, y) = \mathbb{E}(\rho(w_y \star P(\phi_{data}) + b_y)) - \mathbb{E}(\rho(w_y \star P(\phi_x) + b_y))$. We compute the f and angle values by re-sampling ϕ_x ten times (similar to the estimation of FID). When $\tau = 5$ and $\tau = 10$, sometimes we observe a positive angle at $t = T$ in τ -GDA because it oscillates around zero over t .

References

- [1] P.-A. Absil, R Mahony, and Rodolphe Sepulchre. *Optimization Algorithms on Matrix Manifolds*. Princeton University Press, Princeton, 2008.
- [2] El Mehdi Achour, François Malgouyres, and Franck Mamalet. Existence, stability and scalability of orthogonal convolutional neural networks. *Journal of Machine Learning Research*, 23:1–56, jan 2022.
- [3] Waïss Azizian, Ioannis Mitliagkas, Simon Lacoste-Julien, and Gauthier Gidel. A Tight and Unified Analysis of Gradient-Based Methods for a Whole Spectrum of Differentiable Games. In *International Conference on Artificial Intelligence and Statistics*, volume 108 of *Proceedings of Machine Learning Research*, pages 2863–2873, Virtual Event, 2020.
- [4] David Balduzzi, Sebastien Racaniere, James Martens, Jakob Foerster, Karl Tuyls, and Thore Graepel. The Mechanics of n-Player Differentiable Games. In *International Conference on Machine Learning*, volume 80, pages 354–363, Stockholmsmässan, Stockholm Sweden, 2018.
- [5] Gérard Biau, Maxime Sangnier, and Ugo Tanielian. Some theoretical insights into Wasserstein GANs. *Journal of Machine Learning Research*, 22:1–45, 2021.
- [6] Koushik Biswas, Sandeep Kumar, Shilpak Banerjee, and Ashish Kumar Pandey. Smooth Maximum Unit: Smooth Activation Function for Deep Networks using Smoothing Maximum Technique. In *Conference on Computer Vision and Pattern Recognition*, pages 784–793, New Orleans, LA, USA, 2022.
- [7] Nicolas Boumal. *An Introduction to Optimization on Smooth Manifolds*. Cambridge University Press, 2023.
- [8] J Bruna and S Mallat. Invariant Scattering Convolution Networks. *IEEE Transactions on Pattern Analysis and Machine Intelligence*, 35(8):1872–1886, 2013.
- [9] Moustapha Cisse, Piotr Bojanowski, Edouard Grave, Yann Dauphin, and Nicolas Usunier. Parseval networks: improving robustness to adversarial examples. In *International Conference on Machine Learning*, pages 854–863, Sydney, Australia, 2017.
- [10] Constantinos Daskalakis and Ioannis Panageas. The Limit Points of (Optimistic) Gradient Descent in Min-Max Optimization. In *Advances in neural information processing systems*, pages 9256–9266, Red Hook, NY, USA, 2018.
- [11] Étienne de Montbrun and Jérôme Renault. Optimistic Gradient Descent Ascent in Zero-Sum and General-Sum Bilinear Games. *arXiv preprint arXiv:2208.03085*, 2022.
- [12] Tanner Fiez and Lillian J Ratliff. Local convergence analysis of gradient descent ascent with finite timescale separation. In *International Conference on Learning Representation*, 2021.
- [13] Tanner Fiez, Benjamin Chasnov, and Lillian Ratliff. Implicit learning dynamics in stackelberg games: Equilibria characterization, convergence analysis, and empirical study. In *International Conference on Machine Learning*, pages 3133–3144, Virtual Event, 2020. PMLR.
- [14] Ian Gemp and Sridhar Mahadevan. Global Convergence to the Equilibrium of GANs using Variational Inequalities. *arXiv preprint arXiv:1808.01531*, 2018.
- [15] Gauthier Gidel, Hugo Berard, Gaëtan Vignoud, Pascal Vincent, and Simon Lacoste-Julien. A Variational Inequality Perspective on Generative Adversarial Networks. In *International Conference on Learning Representations*, New Orleans, LA, USA, 2019.
- [16] Ishaan Gulrajani, Faruk Ahmed, Martin Arjovsky, Vincent Dumoulin, and Aaron C Courville. Improved training of wasserstein gans. In *Advances in neural information processing systems*, volume 30, pages 5767–5777, Long Beach, CA, USA, 2017.
- [17] Andi Han, Bamdev Mishra, Pratik Jawanpuria, Pawan Kumar, and Junbin Gao. Riemannian Hamiltonian methods for min-max optimization on manifolds. *SIAM Journal on Optimization*, 33(3):1797–1827, 2023.

- [18] Ya-Ping Hsieh, Panayotis Mertikopoulos, and Volkan Cevher. The Limits of Min-Max Optimization Algorithms: Convergence to Spurious Non-Critical Sets. In *International Conference on Machine Learning*, volume 139, pages 4337–4348, Virtual Event, 2021.
- [19] Zihao Hu, Guanghui Wang, Xi Wang, Andre Wibisono, Jacob Abernethy, and Molei Tao. Extragradient Type Methods for Riemannian Variational Inequality Problems. *arXiv preprint arXiv:2309.14155*, 2023.
- [20] Feihu Huang and Shangqian Gao. Gradient Descent Ascent for Minimax Problems on Riemannian Manifolds. *IEEE Transactions on Pattern Analysis and Machine Intelligence*, 1(7):8466 – 8476, 2023.
- [21] Chi Jin, Praneeth Netrapalli, and Michael Jordan. What is local optimality in nonconvex-nonconcave minimax optimization? In *International Conference on Machine Learning*, pages 4880–4889, Virtual Event, 2020.
- [22] Michael Jordan, Tianyi Lin, and Emmanouil-Vasileios Vlatakis-Gkaragkounis. First-Order Algorithms for Min-Max Optimization in Geodesic Metric Spaces. In *Advances in Neural Information Processing Systems*, volume 35, pages 6557–6574, New Orleans, Louisiana, USA, 2022.
- [23] Alistair Letcher, David Balduzzi, Sébastien Racanière, James Martens, Jakob Foerster, Karl Tuyls, and Thore Graepel. Differentiable Game Mechanics. *Journal of Machine Learning Research*, 20(84):1–40, 2019.
- [24] Haochuan Li, Farzan Farnia, Subhro Das, and Ali Jadbabaie. On convergence of gradient descent ascent: A tight local analysis. In *International Conference on Machine Learning*, pages 12717–12740, Baltimore, Maryland USA, 2022. PMLR.
- [25] Tianyi Lin, Chi Jin, and Michael I Jordan. On Gradient Descent Ascent for Nonconvex-Concave Minimax Problems. In *International Conference on Machine Learning*, pages 6083–6093, Virtual Event, 2020.
- [26] Nicolas Loizou, Hugo Berard, Alexia Jolicoeur-Martineau, Pascal Vincent, Simon Lacoste-Julien, and Ioannis Mitliagkas. Stochastic Hamiltonian Gradient Methods for Smooth Games. In *International Conference on Machine Learning*, volume 119, pages 6370–6381, Virtual Event, 2020.
- [27] Pouria Mahdavinia, Yuyang Deng, Haochuan Li, and Mehrdad Mahdavi. Tight analysis of extra-gradient and optimistic gradient methods for nonconvex minimax problems. *Advances in Neural Information Processing Systems*, 35:31213–31225, 2022.
- [28] Jonathan H Manton. Optimization algorithms exploiting unitary constraints. *IEEE Transactions on Signal Processing*, 50(3):635–650, 2002.
- [29] Panayotis Mertikopoulos, Bruno Lecouat, Houssam Zenati, Chuan-Sheng Foo, Vijay Chandrasekhar, and Georgios Piliouras. Optimistic mirror descent in saddle-point problems: Going the extra (gradient) mile. In *International Conference on Learning Representations*, New Orleans, LA, USA, 2019.
- [30] Jan Müller, Reinhard Klein, and Michael Weinmann. Orthogonal wasserstein gans. *arXiv preprint arXiv:1911.13060*, 2019.
- [31] J M Ortega and W C Rheinboldt. *Iterative Solution of Nonlinear Equations in Several Variables*. New York : Academic Press, 1970.
- [32] Edouard Oyallon, Eugene Belilovsky, and Sergey Zagoruyko. Scaling the Scattering Transform: Deep Hybrid Networks. In *International Conference on Computer Vision*, Venice, Italy, 2017.
- [33] Meisam Razaviyayn, Tianjian Huang, Songtao Lu, Maher Nouiehed, Maziar Sanjabi, and Mingyi Hong. Nonconvex min-max optimization: Applications, challenges, and recent theoretical advances. *IEEE Signal Processing Magazine*, 37(5):55–66, 2020.

- [34] Yossi Rubner, Carlo Tomasi, and Leonidas J Guibas. The earth mover’s distance as a metric for image retrieval. *International journal of computer vision*, 40:99–121, 2000.
- [35] W Rudin. *Principles of Mathematical Analysis*. McGraw-Hill Publishing Company, 3rd edition, 1976.
- [36] Maximilian Seitzer. pytorch-fid: FID Score for PyTorch. <https://github.com/mseitzer/pytorch-fid>, 2020.
- [37] Xi Wang, Deming Yuan, Yiguang Hong, Zihao Hu, Lei Wang, and Guodong Shi. Riemannian Optimistic Algorithms. *arXiv preprint arXiv:2308.16004*, 2023.
- [38] Yuanhao Wang, Guodong Zhang, and Jimmy Ba. On Solving Minimax Optimization Locally: A Follow-the-Ridge Approach. In *International Conference on Learning Representations*, Addis Ababa, Ethiopia, 2020.
- [39] Xingzhi Zhan. *Matrix Inequalities*. Springer Berlin, Heidelberg, 2002.
- [40] Guodong Zhang, Yuanhao Wang, Laurent Lessard, and Roger B Grosse. Near-optimal local convergence of alternating gradient descent-ascent for minimax optimization. In *International Conference on Artificial Intelligence and Statistics*, pages 7659–7679, Virtual Event, 2022.
- [41] Peiyuan Zhang, Jingzhao Zhang, and Suvrit Sra. Sion’s Minimax Theorem in Geodesic Metric Spaces and a Riemannian Extragradient Algorithm. *SIAM Journal on Optimization*, 33(4), 2023.

A Implicit function theorem on Riemannian manifold

We state the implicit function theorem in the manifold case which allows one to understand why (x^*, y^*) is a local minimax point. Similar to the local definition of DSE, this theorem implies the existence of a solution $(x, h(x)) \approx (x^*, y^*)$ s.t. $\text{grad}_y f(x, h(x)) = 0$. As a consequence, $h(x)$ is a strict local maximum of $y \mapsto f(x, y)$, thanks to the continuity of $\text{Hess}_y f$ on $\mathcal{M}_1 \times \mathcal{M}_2$ and the continuity of h near x^* (i.e. provided that x is close enough to x^* , we have the positive definiteness of $-\text{Hess}_y f(x, h(x))$).

Denote the set of continuously differentiable vector fields on \mathcal{M}_2 by $\mathcal{X}(\mathcal{M}_2)$. Consider a parameterized vector field ξ defined at each $x \in \mathcal{M}_1$ with $\xi(x, \cdot) \in \mathcal{X}(\mathcal{M}_2)$. Denote the Riemannian connection on \mathcal{M}_2 by ∇_y . By definition, for each $(x, y) \in \mathcal{M}_1 \times \mathcal{M}_2$, $\xi(x, y) \in T_y \mathcal{M}_2$, and $\nabla_y \xi(x, y)$ is a linear map from $T_y \mathcal{M}_2$ to $T_y \mathcal{M}_2$.

Theorem A.1. Assume ξ is continuously differentiable on an open set $E \subset \mathcal{M}_1 \times \mathcal{M}_2$. Let $(x^*, y^*) \in E$ be a solution of

$$\xi(x, y) = 0, \quad (x, y) \in E.$$

If $\nabla_y \xi(x^*, y^*)$ is invertible on $T_{y^*} \mathcal{M}_2$, then there exists an open set $U_1 \times U_2 \subset E$ and an open set $W_1 \subset U_1$ such that

$$\forall x \in W_1, \exists! y \in U_2 \quad \text{s.t.} \quad \xi(x, y) = 0.$$

Let the unique $y = h(x)$, i.e. $h : W_1 \rightarrow U_2$, such that

$$y^* = h(x^*), \quad \xi(x, h(x)) = 0, \quad \forall x \in W_1,$$

then h is continuously differentiable on W_1 . Let $\delta \in T_{x^*} \mathcal{M}_1$, and denote the tangent map of h at x^* by $D_x h(x^*)$, we have

$$D_x h(x^*)[\delta] = -\nabla_y \xi(x^*, y^*)^{-1} \cdot D_x \xi(x^*, y^*)[\delta].$$

The proof is omitted due to its length. The main idea of the proof is similar to that of Theorem 2.1, by using a local coordinate chart around the point (x^*, y^*) to represent a smooth vector field. We then apply the proof technique of the implicit function theorem in Euclidean space [35, Theorem 9.28].

B Proof of Theorem 2.1

Let $\mathcal{X}(\mathcal{M}_1)$ (resp. $\mathcal{X}(\mathcal{M}_2)$) be the set of continuously differentiable vector fields on \mathcal{M}_1 (resp. \mathcal{M}_2). Since f is twice continuously differentiable, we have for any $y \in \mathcal{M}_2$ (resp. $x \in \mathcal{M}_1$), $\text{grad}_x f(\cdot, y) \in \mathcal{X}(\mathcal{M}_1)$ (resp. $\text{grad}_y f(x, \cdot) \in \mathcal{X}(\mathcal{M}_2)$).

To show that the local definition of DSE is equivalent to its intrinsic definition, we shall write the Riemannian gradients $\text{grad}_x f(x, y)$ and $\text{grad}_y f(x, y)$ in the local coordinate chart $(O_1 \times O_2, \varphi_1 \times \varphi_2)$. We write g_1 and g_2 to denote the Riemannian metric on \mathcal{M}_1 and \mathcal{M}_2 .

For each $x \in O_1$ (resp. $y \in O_2$), let $\{E_{1,i}(x)\}_{i \leq d_1}$ (resp. $\{E_{2,j}(y)\}_{j \leq d_2}$) be the canonical basis of the tangent space $T_x \mathcal{M}_1$ (resp. $T_y \mathcal{M}_2$), defined by the tangent map $D\varphi_1^{-1}(\varphi_1(x))[e_{1,i}]$ of the canonical basis $\{e_{1,i}\}_{i \leq d_1}$ on \mathbb{R}^{d_1} (resp. $D\varphi_2^{-1}(\varphi_2(y))[e_{2,j}]$ of $\{e_{2,j}\}_{j \leq d_2}$ on \mathbb{R}^{d_2}).

Let the local coordinate of $(x, y) \in O_1 \times O_2$ be $(u_1, u_2) = (\varphi_1(x), \varphi_2(y)) \in \bar{O}_1 \times \bar{O}_2 = \varphi_1(O_1) \times \varphi_2(O_2) \subset \mathbb{R}^{d_1} \times \mathbb{R}^{d_2}$. We can represent

$$\xi_1(x, y) = \text{grad}_x f(x, y) = \sum_{i \leq d_1} \xi_{1,i}(x, y) E_{1,i}(x), \quad (15)$$

$$\xi_2(x, y) = \text{grad}_y f(x, y) = \sum_{j \leq d_2} \xi_{2,j}(x, y) E_{2,j}(y). \quad (16)$$

From (15) and (16), the local coordinates of the Riemannian gradients on $\bar{O}_1 \times \bar{O}_2$ are

$$\bar{\xi}_1(u_1, u_2) = \sum_{i \leq d_1} \xi_{1,i}(\varphi_1^{-1}(u_1), \varphi_2^{-1}(u_2)) e_{1,i}, \quad (17)$$

$$\bar{\xi}_2(u_1, u_2) = \sum_{j \leq d_2} \xi_{2,j}(\varphi_1^{-1}(u_1), \varphi_2^{-1}(u_2)) e_{2,j}. \quad (18)$$

Equivalence between (1) and (4) Let the local Riemannian metric matrix at $x = \varphi_1^{-1}(u_1) \in O_1$ and $y = \varphi_2^{-1}(u_2) \in O_2$ be

$$\bar{g}_1(u_1) = (g_1(E_{1,i}(x), E_{1,i'}(x)))_{i,i' \leq d_1}, \quad \bar{g}_2(u_2) = (g_2(E_{2,j}(y), E_{2,j'}(y)))_{j,j' \leq d_2}. \quad (19)$$

From [1, chap. 3.6], we have for $(u_1, u_2) \in \bar{O}_1 \times \bar{O}_2$,

$$\bar{\xi}_1(u_1, u_2) = \bar{g}_1(u_1)^{-1} \cdot \partial_{u_1} \bar{f}(u_1, u_2), \quad (20)$$

$$\bar{\xi}_2(u_1, u_2) = \bar{g}_2(u_2)^{-1} \cdot \partial_{u_2} \bar{f}(u_1, u_2). \quad (21)$$

The equivalence between the DSE condition (1) and (4) follows from (20) and (21), as $\bar{\xi}_1(u_1^*, u_2^*) = 0$ i.f.f. (if and only if) $\text{grad}_x f(x^*, y^*) = 0$ (similarly for the relationship between ξ_2 and $\text{grad}_y f$).

Equivalence between (2) and (5) Let $\eta^* \in T_{y^*} \mathcal{M}_2$, with its local coordinate $\bar{\eta}^* = D\varphi_2(y^*)[\eta^*]$. To show that the positive definiteness of $-\text{Hess}_y f(x^*, y^*)$ is equivalent to the positive definiteness of $-\partial_{u_2 u_2}^2 \bar{f}(u_1^*, u_2^*)$, it is sufficient to verify that

$$\langle \bar{\eta}^*, \partial_{u_2 u_2}^2 \bar{f}(u_1^*, u_2^*) \bar{\eta}^* \rangle = \langle \eta^*, \text{Hess}_y f(x^*, y^*)[\eta^*] \rangle_{y^*}, \quad (22)$$

where $\langle \cdot, \cdot \rangle$ denotes the inner product on Euclidean space, and $\langle \cdot, \cdot \rangle_{y^*}$ denotes the Riemannian inner product on $T_{y^*} M$.

Recall that the Riemannian Hessian on \mathcal{M}_2 is defined by the Riemannian connection $\nabla_y : \mathcal{X}(\mathcal{M}_2) \times \mathcal{X}(\mathcal{M}_2) \rightarrow \mathcal{X}(\mathcal{M}_2)$ with $\text{Hess}_y f(x, y) = \nabla_y \xi_2(x, y)$. By the *R-linearity* and *Leibniz law* of the connection, we have

$$\begin{aligned} \nabla_y \xi_2(x^*, y^*)[\eta^*] &= \nabla_y \left(\sum_j \xi_{2,j}(x^*, y^*) E_{2,j}(y^*) \right) [\eta^*] \\ &= \sum_j \nabla_y (\xi_{2,j}(x^*, y^*) E_{2,j}(y^*)) [\eta^*] \\ &= \sum_j (D_y \xi_{2,j}(x^*, y^*)[\eta^*] E_{2,j}(y^*) + \xi_{2,j}(x^*, y^*) \nabla_y (E_{2,j}(y^*)) [\eta^*]) \\ &= \sum_j \left(\frac{\partial \bar{\xi}_{2,j}}{\partial u_2}(u_1^*, u_2^*) \bar{\eta}^* \right) E_{2,j}(y^*). \end{aligned} \quad (23)$$

$$= \sum_j \left(\frac{\partial \bar{\xi}_{2,j}}{\partial u_2}(u_1^*, u_2^*) \bar{\eta}^* \right) E_{2,j}(y^*). \quad (24)$$

We have obtained (24) from (23) because any DSE (x^*, y^*) is a stationary point of f , therefore $\xi_{2,j}(x^*, y^*) = 0$ for each $j \leq d_2$. Moreover, the tangent map $D_y \xi_{2,j}(x^*, y^*)[\eta^*] = \frac{\partial \bar{\xi}_{2,j}}{\partial u_2}(u_1^*, u_2^*) \bar{\eta}^*$ by definition [1, chap. 3.5.4].

Therefore the local coordinate of the tangent vector $\nabla_y \xi_2(x^*, y^*)[\eta^*] \in T_{y^*} \mathcal{M}_2$ is $\frac{\partial \bar{\xi}_2}{\partial u_2}(u_1^*, u_2^*) \bar{\eta}^* \in \mathbb{R}^{d_2}$. It follows from (21), (24), and the Riemannian inner product [1, chap. 3.6] that

$$\begin{aligned} \langle \eta^*, \text{Hess}_y f(x^*, y^*)[\eta^*] \rangle_{y^*} &= \left\langle \bar{\eta}^*, \bar{g}_2(u_2^*) \cdot \frac{\partial \bar{\xi}_2}{\partial u_2}(u_1^*, u_2^*) \bar{\eta}^* \right\rangle \\ &= \langle \bar{\eta}^*, \partial_{u_2 u_2}^2 \bar{f}(u_1^*, u_2^*) \bar{\eta}^* \rangle. \end{aligned} \quad (25)$$

Therefore (22) holds. This verifies the equivalence between (2) and (5).

Equivalence between (3) and (6) Assume (x^*, y^*) is a DSE of f , from the equivalence between (1), (2) and (4), (5), we deduce that (x^*, y^*) (resp. (u_1^*, u_2^*)) is a stationary point of f (resp. \bar{f}). Moreover, $\text{Hess}_y f(x^*, y^*)$ and $\partial_{u_2 u_2}^2 \bar{f}(u_1^*, u_2^*)$ are negative definite.

To simplify the notation, let

$$A = -\partial_{u_2 u_2}^2 \bar{f}(u_1^*, u_2^*), \quad B = \partial_{u_2 u_1}^2 \bar{f}(u_1^*, u_2^*), \quad C = \partial_{u_1 u_1}^2 \bar{f}(u_1^*, u_2^*). \quad (26)$$

The condition (3) is equivalent to the positive definiteness of the matrix $C + BA^{-1}B^\top$.

Let $\delta^* \in T_{x^*} \mathcal{M}_1$, with its local coordinate $\bar{\delta}^* = D\varphi_1(x^*)[\delta^*]$. As in (22), it suffices to verify that

$$\langle \bar{\delta}^*, (C + BA^{-1}B^\top) \bar{\delta}^* \rangle = \langle \delta^*, [\text{Hess}_x f - \text{grad}_{y^*}^2 f \cdot (\text{Hess}_y f)^{-1} \cdot \text{grad}_{x^*}^2 f](x^*, y^*)[\delta^*] \rangle_{x^*}.$$

Based on the proof of (22), we also have $\langle \bar{\delta}^*, C\bar{\delta}^* \rangle = \langle \delta^*, \text{Hess}_x f(x^*, y^*)[\delta^*] \rangle_{x^*}$. It remains to verify that

$$\langle \bar{\delta}^*, BA^{-1}B^\top \bar{\delta}^* \rangle = \langle \delta^*, [-\text{grad}_{yx}^2 f \cdot (\text{Hess}_y f)^{-1} \cdot \text{grad}_{xy}^2 f](x^*, y^*)[\delta^*] \rangle_{x^*}. \quad (27)$$

Let $\eta^* = [\text{Hess}_y f^{-1} \cdot \text{grad}_{xy}^2 f](x^*, y^*)[\delta^*]$, we compute the local coordinate $\bar{\eta}^*$ of η^* by converting the following equation

$$\text{Hess}_y f(x^*, y^*)[\eta^*] = \text{grad}_{xy}^2 f(x^*, y^*)[\delta^*], \quad (28)$$

into local coordinate. From (24), we have $\text{Hess}_y f(x^*, y^*)[\eta^*] = \sum_j \left(\frac{\partial \bar{\xi}_{2,j}}{\partial u_2}(u_1^*, u_2^*) \bar{\eta}^* \right) E_{2,j}(y^*)$.

By (16) and (18), we obtain

$$\begin{aligned} \text{grad}_{xy}^2 f(x^*, y^*)[\delta^*] &= D_x \text{grad}_y f(x^*, y^*)[\delta^*] = \sum_j D_x \xi_{2,j}(x^*, y^*)[\delta^*] E_{2,j}(y^*) \\ &= \sum_j \left(\frac{\partial \bar{\xi}_{2,j}}{\partial u_1}(u_1^*, u_2^*) \bar{\delta}^* \right) E_{2,j}(y^*). \end{aligned} \quad (29)$$

It follows that (28) is equivalent to

$$\frac{\partial \bar{\xi}_2}{\partial u_2}(u_1^*, u_2^*) \bar{\eta}^* = \frac{\partial \bar{\xi}_2}{\partial u_1}(u_1^*, u_2^*) \bar{\delta}^*. \quad (30)$$

We can compute the right hand side of (27) in the local coordinate as in (29) and (25),

$$\begin{aligned} \langle \delta^*, -\text{grad}_{yx}^2 f(x^*, y^*)[\eta^*] \rangle_{x^*} &= -\langle \delta^*, D_y \text{grad}_x f(x^*, y^*)[\eta^*] \rangle_{x^*} \\ &= -\left\langle \delta^*, \sum_i \left(\frac{\partial \bar{\xi}_{1,i}}{\partial u_2}(u_1^*, u_2^*) \bar{\eta}^* \right) E_{1,i}(x^*) \right\rangle_{x^*} \\ &= -\left\langle \bar{\delta}^*, \bar{g}_1(u_1^*) \cdot \frac{\partial \bar{\xi}_1}{\partial u_2}(u_1^*, u_2^*) \bar{\eta}^* \right\rangle. \end{aligned}$$

The left hand side of (27) can be computed based on (20) and (21), which results in

$$A = -\bar{g}_2(u_2^*) \cdot \frac{\partial \bar{\xi}_2}{\partial u_2}(u_1^*, u_2^*), \quad (31)$$

$$B = \bar{g}_1(u_1^*) \cdot \frac{\partial \bar{\xi}_1}{\partial u_2}(u_1^*, u_2^*), \quad (32)$$

$$C = \bar{g}_1(u_1^*) \cdot \frac{\partial \bar{\xi}_1}{\partial u_1}(u_1^*, u_2^*).$$

Furthermore, the symmetry of the Hessian matrix of \bar{f} implies that

$$B^\top = \partial_{u_1 u_2}^2 \bar{f}(u_1^*, u_2^*) = \bar{g}_2(u_2^*) \cdot \frac{\partial \bar{\xi}_2}{\partial u_1}(u_1^*, u_2^*). \quad (33)$$

As a consequence, (30) implies that $\bar{\eta}^* = -A^{-1}B^\top \bar{\delta}^*$, and

$$\langle \bar{\delta}^*, BA^{-1}B^\top \bar{\delta}^* \rangle = -\left\langle \bar{\delta}^*, \bar{g}_1(u_1^*) \cdot \frac{\partial \bar{\xi}_1}{\partial u_2}(u_1^*, u_2^*) \bar{\eta}^* \right\rangle.$$

Therefore (27) holds.

C Proof of Proposition 2.1

We verify the intrinsic definition of DSE for (x^*, y^*) . For the first-order condition in (4), we compute based on [7, Proposition 3.61],

$$\partial_x f(x, y) = A^\top y, \quad \text{grad}_y f(x, y) = (I - yy^\top)(Ax - b). \quad (34)$$

From the identity involving the pseudo-inverse $A^\top A A^+ = A^\top$, we deduce that $A^\top y^* = 0$. As $b \notin \text{Range}(A)$, we have $Ax^* - b \neq 0$ and therefore y^* is parallel to the (non-zero) vector $Ax^* - b$. From above, the first-order condition holds, i.e. $\partial_x f(x^*, y^*) = 0$, $\text{grad}_y f(x^*, y^*) = 0$.

From (34), we first verify the second-order condition (5). From [7, Corollary 5.16], we compute for $\eta \in T_y \mathcal{M}_2$,

$$\begin{aligned} \text{Hess}_y f(x, y)[\eta] &= (I - yy^\top)(\langle \partial_y \text{grad}_y f(x, y), \eta \rangle) \\ &= (I - yy^\top)(-(y\eta^\top + \eta y^\top)(Ax - b)) \\ &= \langle y, Ax - b \rangle(-\eta). \end{aligned}$$

We verify that $-\text{Hess}_y f(x^*, y^*)$ is d.p, because for non-zero $\eta^* \in T_{y^*} \mathcal{M}_2$, we have $\|\eta^*\|^2 > 0$. Moreover, $Ax^* - b \neq 0$, therefore

$$\langle -\text{Hess}_y f(x^*, y^*)[\eta^*], \eta^* \rangle = \langle y^*, Ax^* - b \rangle \|\eta^*\|^2 = \|Ax^* - b\| \|\eta^*\|^2 > 0.$$

We now check the second-order condition (6). It is clear that $\partial_{xx}^2 f(x, y) = 0$. We next show $\delta^* \mapsto \text{grad}_{xy}^2 f(x^*, y^*)[\delta^*]$ is an injection from $T_{x^*} \mathcal{M}_1$ to $T_{y^*} \mathcal{M}_2$. We compute from (34),

$$\text{grad}_{xy}^2 f(x^*, y^*)[\delta^*] = \sum_{i \leq d_1} \partial_{x_i} \text{grad}_y f(x^*, y^*) \delta_i^* = (I - y^* y^{*\top}) A \delta^*.$$

If $\delta^* \neq 0$, then $A\delta^* \neq 0$ because $\text{Ker}(A) = \{0\}$. But $A\delta^*$ is not parallel to y^* , since y^* is along the direction $Ax^* - b$ which is not in the range of A . This proves that $\text{grad}_{xy}^2 f(x^*, y^*)[\delta^*] \neq 0$ if $\delta^* \neq 0$.

The above injection property implies that for $\delta^* \neq 0$, $\eta^* = \text{grad}_{xy}^2 f(x^*, y^*)[\delta^*] \neq 0$. As $-\text{Hess}_y f(x^*, y^*)$ is d.p, we use the symmetry of the Riemannian cross-gradients (see Proposition I.1) to obtain: If $\delta^* \neq 0$, then

$$\langle \delta^*, [\text{Hess}_x f - \text{grad}_{xy}^2 f \cdot (\text{Hess}_y f)^{-1} \cdot \text{grad}_{xy}^2 f](x^*, y^*)[\delta^*] \rangle = \langle \eta^*, -\text{Hess}_y f(x^*, y^*)^{-1}[\eta^*] \rangle > 0.$$

Therefore (6) holds.

D Proof of Proposition 2.2

As in the proof of Proposition 2.1 in Appendix C, we have

$$\partial_x f(x, y) = A^\top y - \kappa A^\top Ax, \quad \text{grad}_y f(x, y) = (I - yy^\top)(Ax - b). \quad (35)$$

To show the existence of DSE, we shall construct a solution of the form (x, y_x^*) , where $\partial_x f(x, y_x^*) = 0$. We consider $y_x^* = (Ax - b)/\|Ax - b\|$ so that $\text{grad}_y f(x, y_x^*) = 0$. We verify that $\text{Ker}(A) = \{0\}$ implies that $A^\top A$ is p.d. It follows that $A^+ = (A^\top A)^{-1} A^\top$, and that the condition $\partial_x f(x, y_x^*) = 0$ is equivalent to

$$\frac{A^\top (Ax - b)}{\|Ax - b\|} = \kappa A^\top Ax \quad \Leftrightarrow \quad (1 - \kappa \|Ax - b\|)x = A^+ b.$$

For $(x^*, y^*) = (x^*, y_{x^*}^*)$ to be a DSE, we assume $x^* = cA^+b$ and we want to find a $c \in \mathbb{R}$ such that

$$F(\kappa, c) = c(1 - \kappa \|cAA^+b - b\|) - 1 = 0.$$

From Proposition 2.1, we have $F(0, 1) = 0$. We next apply the implicit function theorem (c.f. Theorem A.1) to show the existence of c close to 1 if κ is close to 0. It suffices to verify that $\frac{\partial F}{\partial c}(0, 1) = 1$ based on

$$\frac{\partial F}{\partial c}(\kappa, c) = (1 - \kappa \|cAA^+b - b\|) + c \left(-\kappa \frac{\langle AA^+b, cAA^+b - b \rangle}{\|cAA^+b - b\|} \right).$$

This suggests that there is an implicit function h defined on an open neighbor W_1 of $\kappa = 0$ ($0 \in W_1$) such that $F(\kappa, h(\kappa)) = 0$. Moreover, $h(0) = 1$. We next check that if $c = h(\kappa)$ for some range $0 < \kappa < \kappa_0$, then (x^*, y^*) defined in the statement is a DSE of f . Since (35) hold at (x^*, y^*) , it suffices to verify the second-order condition of DSE.

We verify the second-order condition (5) by using the same proof of Proposition 2.1. To check the second-order condition (6), we first compute from (35)

$$\eta^* = \text{grad}_{xy}^2 f(x^*, y^*)[\delta^*] = \sum_{i \leq d_1} \partial_{x_i} \text{grad}_y f(x^*, y^*) \delta_i^* = (I - y^* y^{*\top}) A \delta^*.$$

By following the proof of Proposition 2.1, we then compute

$$\begin{aligned} S(\kappa) &= \langle \delta^*, [\text{Hess}_x f - \text{grad}_{yx}^2 f \cdot (\text{Hess}_y f)^{-1} \cdot \text{grad}_{xy}^2 f](x^*, y^*)[\delta^*] \rangle \\ &= -\kappa \|A \delta^*\|^2 + \langle \eta^*, -\text{Hess}_y f(x^*, y^*)^{-1}[\eta^*] \rangle \\ &= -\kappa \|A \delta^*\|^2 + \frac{1}{\|Ax^* - b\|} \|\eta^*\|^2. \end{aligned}$$

It is clear that $S(\kappa)$ is a continuous function of κ because $x^* = h(\kappa)A^+b$ and $y^* = (Ax^* - b)/\|Ax^* - b\|$ are continuous with respect to κ . Moreover, $S(0) > 0$ from the proof of Proposition 2.1 (due to the injection property of $\delta^* \mapsto \text{grad}_{xy}^2 f(x^*, y^*)[\delta^*]$). Therefore there exists $\kappa_0 > 0$ so that $S(\kappa) > 0$ for $0 < \kappa < \kappa_0$ (i.e. (6) holds).

E Proof of Proposition 2.3

We verify the intrinsic definition of DNE for (x^*, y^*) . For the first-order condition (7), we compute

$$\partial_x f(x, y) = A^\top(Ax + y - b), \quad \text{grad}_y f(x, y) = (I - yy^\top)(Ax + y - b). \quad (36)$$

From the identity involving the pseudo-inverse $A^\top AA^+ = A^\top$, we deduce that $A^\top(Ax^* + y^* - b) = 0$. As $b \notin \text{Range}(A)$, we have $Ax^* - b \neq 0$ and therefore y^* is parallel to the vector $Ax^* - b$. From above, the first-order condition in (4) holds.

From (36), we next verify the second-order condition (8). It is clear that $\partial_{xx}^2 f(x, y) = A^\top A$ is p.d. From [7, Corollary 5.16], we compute for $\eta \in T_y \mathcal{M}_2$,

$$\begin{aligned} \text{Hess}_y f(x, y)[\eta] &= (I - yy^\top)(\langle \partial_y \text{grad}_y f(x, y), \eta \rangle) \\ &= (I - yy^\top)(\eta - (y\eta^\top + \eta y^\top)(Ax + y - b)) \\ &= \eta(1 - \langle y, Ax + y - b \rangle) \\ &= \langle y, Ax - b \rangle(-\eta). \end{aligned}$$

We verify that $-\text{Hess}_y f(x^*, y^*)$ is d.p, because for non-zero $\eta^* \in T_{y^*} \mathcal{M}_2$, we have $\|\eta^*\|^2 > 0$. Moreover, $Ax^* - b \neq 0$, therefore

$$\langle -\text{Hess}_y f(x^*, y^*)[\eta^*], \eta^* \rangle = \langle y^*, Ax^* - b \rangle \|\eta^*\|^2 = \|Ax^* - b\| \|\eta^*\|^2 > 0.$$

Therefore (8) holds.

F Proof of Theorem 3.1

It remains to prove that the spectral radius of the Jacobian matrix $\bar{\mathbf{T}}'(u_1^*, u_2^*)$ is strictly smaller than one, we shall first compute this matrix $\bar{\mathbf{T}}'(u_1^*, u_2^*)$, and then relate it to $\mathbf{T}'(x^*, y^*)$.

First of all, we specify the induced dynamics $\bar{\mathbf{T}}$ of \mathbf{T} by using the local coordinate representation of the retractions \mathcal{R}_1 and \mathcal{R}_2 near the stationary point (x^*, y^*) . Let $(O_1 \times O_2, \varphi_1 \times \varphi_2)$ be the local chart. Since a retraction [1, Section 4.1] is a smooth function from the tangent bundle of a manifold to the manifold itself, we can identify an open subset B_1 of the tangent bundle of \mathcal{M}_1 (similarly on B_2 for \mathcal{M}_2) such that $x \in O_1$ and $\mathcal{R}_{1,x}(\xi_1) \in O_1$ if $(x, \xi_1) \in B_1$. This set B_1 can then be mapped to an open set $\bar{B}_1 \subset \mathbb{R}^{d_1} \times \mathbb{R}^{d_1}$, using the local chart of the tangent bundle ([1, Section 3.5.3]). On this subset \bar{B}_1 , we can define the local representation of \mathcal{R}_1 as follows

$$\bar{\mathcal{R}}_1 : \bar{B}_1 \rightarrow \bar{O}_1, \quad \bar{\mathcal{R}}_1(u_1, \bar{\xi}_1) = \varphi_1 \circ \mathcal{R}_{1, \varphi_1^{-1}(u_1)}(D\varphi_1^{-1}(u_1)[\bar{\xi}_1]),$$

Similarly for \mathcal{R}_2 , we can define $\bar{\mathcal{R}}_2 : \bar{B}_2 \rightarrow \bar{O}_2$ on an open set $\bar{B}_2 \subset \mathbb{R}^{d_2} \times \mathbb{R}^{d_2}$. From the above definition of $\bar{\mathcal{R}}_1$ and $\bar{\mathcal{R}}_2$, as well as the local coordinate of $\xi_1(x, y)$ and $\xi_2(x, y)$ (as in (17),(18)), we obtain the induced dynamics

$$\bar{\mathbf{T}}(u_1, u_2) = \begin{pmatrix} \bar{\mathcal{R}}_1(u_1, \bar{\xi}_1(u_1, u_2)) \\ \bar{\mathcal{R}}_2(u_2, \bar{\xi}_2(u_1, u_2)) \end{pmatrix}, \quad (37)$$

which is well defined on the non-empty open set $\{(u_1, u_2) \in \bar{O}_1 \times \bar{O}_2 | (u_1, \bar{\xi}_1(u_1, u_2)) \in \bar{B}_1, (u_2, \bar{\xi}_2(u_1, u_2)) \in \bar{B}_2\}$.

From (37), we can compute the Jacobian matrix $\bar{\mathbf{T}}'(u_1^*, u_2^*)$ using the chain rule. As $\bar{\xi}_1(u_1^*, u_2^*) = 0$ and $\bar{\xi}_2(u_1^*, u_2^*) = 0$, we have

$$\bar{\mathbf{T}}'(u_1^*, u_2^*) = \begin{pmatrix} I_{d_1} + \frac{\partial \bar{\xi}_1}{\partial u_1}(u_1^*, u_2^*) & \frac{\partial \bar{\xi}_1}{\partial u_2}(u_1^*, u_2^*) \\ \frac{\partial \bar{\xi}_2}{\partial u_1}(u_1^*, u_2^*) & I_{d_2} + \frac{\partial \bar{\xi}_2}{\partial u_2}(u_1^*, u_2^*) \end{pmatrix}, \quad (38)$$

since the retraction by definition satisfies $\frac{\partial \bar{\mathcal{R}}_1}{\partial u_1}(u_1^*, 0) = I_{d_1}$, $\frac{\partial \bar{\mathcal{R}}_1}{\partial \xi_1}(u_1^*, 0) = I_{d_1}$ (similarly for $\bar{\mathcal{R}}_2$).

We next verify that eigenvalues of the matrix in (38) are the same as $\mathbf{T}'(x^*, y^*)$. Let $\delta^* = \sum_i \bar{\delta}_i^* E_{1,i}(x^*) \in T_{x^*} \mathcal{M}_1$, $\eta^* = \sum_j \bar{\eta}_j^* E_{2,j}(y^*) \in T_{y^*} \mathcal{M}_2$, then following the same argument as in (24) and (29), we have

$$\begin{aligned} \nabla_x \xi_1(x^*, y^*)[\delta^*] &= \sum_{i=1}^{d_1} \left(\frac{\partial \bar{\xi}_{1,i}}{\partial u_1}(u_1^*, u_2^*) \bar{\delta}^* \right) E_{1,i}(x^*), \\ D_y \xi_1(x^*, y^*)[\eta^*] &= \sum_{i=1}^{d_1} \left(\frac{\partial \bar{\xi}_{1,i}}{\partial u_2}(u_1^*, u_2^*) \bar{\eta}^* \right) E_{1,i}(x^*), \\ D_x \xi_2(x^*, y^*)[\delta^*] &= \sum_{j=1}^{d_2} \left(\frac{\partial \bar{\xi}_{2,j}}{\partial u_1}(u_1^*, u_2^*) \bar{\delta}^* \right) E_{2,j}(y^*), \\ \nabla_y \xi_2(x^*, y^*)[\eta^*] &= \sum_{j=1}^{d_2} \left(\frac{\partial \bar{\xi}_{2,j}}{\partial u_2}(u_1^*, u_2^*) \bar{\eta}^* \right) E_{2,j}(y^*). \end{aligned}$$

From the definition of eigenvalue and eigenvector pairs, these equations indicate that their eigenvalues are indeed the same.

G Proof of Theorem 3.2

Let $\bar{\mathbf{T}}'(u_1^*, u_2^*) = I_{d_1+d_2} + \gamma M$. We show that the real part of each eigenvalue of M is strictly smaller than zero. From this, we can set $\gamma^\bullet = -2 \max_k \frac{\text{Re}(\lambda_k(M))}{|\lambda_k(M)|^2} > 0$ and check that if $0 < \gamma < \gamma^\bullet$, the spectral radius of $\bar{\mathbf{T}}'(u_1^*, u_2^*)$ is strictly smaller than one.

From (38) and (31)-(33), the M matrix is given by

$$M = \begin{pmatrix} -\bar{g}_1(u_1^*)^{-1} \cdot C & -\bar{g}_1(u_1^*)^{-1} \cdot B \\ \tau \bar{g}_2(u_2^*)^{-1} \cdot B^\top & -\tau \bar{g}_2(u_2^*)^{-1} \cdot A \end{pmatrix},$$

where the matrices A, B, C are defined in (26). To analyze the eigenvalue of M , we could not apply [24, Lemma 5.2] to the matrix M since the local metric $\bar{g}_1(u_1^*)$ and $\bar{g}_2(u_2^*)$ are not identity matrices. We consider a matrix $\bar{\mathbf{M}}$ which is similar to M so that they have the same eigenvalues,

$$\bar{\mathbf{M}} = \begin{pmatrix} -\bar{\mathbf{C}} & -\bar{\mathbf{B}} \\ \tau \bar{\mathbf{B}}^\top & -\tau \bar{\mathbf{A}} \end{pmatrix} \quad (39)$$

where

- $\bar{\mathbf{C}} = \bar{g}_1(u_1^*)^{-1/2} \cdot C \cdot \bar{g}_1(u_1^*)^{-1/2}$
- $\bar{\mathbf{B}} = \bar{g}_1(u_1^*)^{-1/2} \cdot B \cdot \bar{g}_2(u_2^*)^{-1/2}$
- $\bar{\mathbf{A}} = \bar{g}_2(u_2^*)^{-1/2} \cdot A \cdot \bar{g}_2(u_2^*)^{-1/2}$

We first check that the following conditions hold:

- $\bar{\mathbf{A}}$ is p.d because A is p.d.
- $\bar{\mathbf{C}} + \bar{\mathbf{B}} \bar{\mathbf{A}}^{-1} \bar{\mathbf{B}}^\top$ is p.d because $C + B A^{-1} B^\top$ is p.d.

- $\tau > \|\bar{\mathbf{C}}\|/\lambda_{\min}(\bar{\mathbf{A}})$.

Indeed, we can relate these conditions to the following intrinsic quantities on the manifold $\mathcal{M}_1 \times \mathcal{M}_2$, by following the proof of Theorem 2.1 (see Appendix B):

- Let $\mathbf{A} = -\text{Hess}_y f(x^*, y^*)$, then \mathbf{A} and $\bar{\mathbf{A}}$ have the same eigenvalues.
- Let $\mathbf{B} = \text{grad}_{yx}^2 f(x^*, y^*)$, $\mathbf{B}^\top = \text{grad}_{xy}^2 f(x^*, y^*)$, then $\mathbf{C} + \mathbf{B}\mathbf{A}^{-1}\mathbf{B}^\top$ and $\bar{\mathbf{C}} + \bar{\mathbf{B}}\bar{\mathbf{A}}^{-1}\bar{\mathbf{B}}^\top$ have the same eigenvalues.
- Let $\mathbf{C} = \text{Hess}_x f(x^*, y^*)$, then \mathbf{C} and $\bar{\mathbf{C}}$ have the same eigenvalues.
- The condition $\tau > \max_k |\lambda_k(\mathbf{C})|/\lambda_{\min}(\mathbf{A})$ implies that $\tau > \|\bar{\mathbf{C}}\|/\lambda_{\min}(\bar{\mathbf{A}})$.

G.1 Spectral analysis of \mathbf{M}

To analyze the eigenvalue of \mathbf{M} , we use the next proposition which is adapted from [24, Lemma 5.2] with a refined range of τ . For two real symmetric matrices A and B , we write $A \geq B$ if $A - B$ is semi-p.d. We write $A > B$ if $A - B$ is p.d. For a symmetric matrix A , $\lambda_{\max}(A)$ denotes the maximal eigenvalue of A , and $\lambda_{\min}(A)$ denotes the minimal eigenvalue of A .

Proposition G.1. *Let $A \in \mathbb{R}^{m \times m}$, $B \in \mathbb{R}^{n \times m}$, $C \in \mathbb{R}^{n \times n}$ such that A and $C + \mathbf{B}\mathbf{A}^{-1}\mathbf{B}^\top$ are positive definite. Assume that $\tau > \|C\|/\lambda_{\min}(A)$, then any eigenvalue $\lambda = \lambda_0 + i\lambda_1$ (with $\lambda_0 \in \mathbb{R}, \lambda_1 \in \mathbb{R}$) of the following matrix,*

$$M = \begin{pmatrix} -C & -B \\ \tau B^\top & -\tau A \end{pmatrix}$$

satisfies $\lambda_0 < 0$.

Proof. We show that $\lambda_0 \geq 0$ will lead to a contradiction, by following the proof of [24, Lemma 5.2]. Assume that λ is an eigenvalue of M , i.e. $\det(\lambda I - M) = 0$. To compute $\det(\lambda I - M)$, notice that $\lambda I + \tau A$ is invertible since $\lambda_0 I + \tau A$ is positive definite (A is positive definite and $\lambda_0 \geq 0$). By the Schur complement, we have

$$\begin{aligned} \det(\lambda I - M) &= \det \begin{pmatrix} C + \lambda I & B \\ -\tau B^\top & \tau A + \lambda I \end{pmatrix} \\ &= \det(\lambda I + \tau A) \det(H(\lambda)) \end{aligned} \quad (40)$$

where $H(\lambda) = \lambda I + C + B(\lambda/\tau + A)^{-1}\mathbf{B}^\top$. As $\lambda I + \tau A$ is invertible, $\det(\lambda I - M) = 0$ implies that $\det(H(\lambda)) = 0$.

Let the spectral decomposition of A be $U\Lambda_A U^\top$, with orthogonal $U \in \mathbb{R}^{m \times m}$ and diagonal $\Lambda_A = \text{diag}(\lambda_1(A), \dots, \lambda_m(A)) \in \mathbb{R}^{m \times m}$. Then

$$H(\lambda) = \lambda I + C + \tilde{B}D\tilde{B}^\top,$$

with $\tilde{B} = BU$ and $D = \text{diag}(d_1, \dots, d_m)$ where

$$d_k = \frac{1}{\lambda/\tau + \lambda_k(A)} = \frac{\lambda_0/\tau + \lambda_k(A) - i\lambda_1/\tau}{(\lambda_0/\tau + \lambda_k(A))^2 + (\lambda_1/\tau)^2}, \quad 1 \leq k \leq m.$$

It follows that if $\lambda_0 > \|C\|$, then the real-part of $H(\lambda)$ is

$$\text{Re}(H(\lambda)) = \lambda_0 I + C + \tilde{B}\text{Re}(D)\tilde{B}^\top \quad \text{p.d.} \quad (41)$$

This is contradictory to the fact that $\det(H(\lambda)) = 0$ [24, Corollary 10.2]. On the other hand, if $0 \leq \lambda_0 \leq \|C\|$ and $\lambda_1 \neq 0$, then consider for $\beta \in \mathbb{R}$,

$$\begin{aligned} \text{Re}(H(\lambda)) + \frac{\tau\beta}{\lambda_1} \text{Im}(H(\lambda)) &= \lambda_0 I + C + \tilde{B}\text{Re}(D)\tilde{B}^\top + \frac{\tau\beta}{\lambda_1} (\lambda_1 I + \tilde{B}\text{Im}(D)\tilde{B}^\top) \\ &= (\lambda_0 + \tau\beta)I + C + \tilde{B}F\tilde{B}^\top, \end{aligned} \quad (42)$$

where $F = \text{diag}(f_1, \dots, f_m)$ with

$$f_k = \frac{\lambda_0/\tau + \lambda_k(A) - \beta}{(\lambda_0/\tau + \lambda_k(A))^2 + (\lambda_1/\tau)^2}, \quad 1 \leq k \leq m. \quad (43)$$

Take $\beta = \lambda_{\min}(A)$, then $f_k \geq 0$ for each $k \leq m$. The condition $\tau\lambda_{\min}(A) > \|C\|$ implies $(\lambda_0 + \tau\beta)I + C$ is p.d. and together with (43), we have (42) is p.d., so it is contradictory to the fact that $\det(H(\lambda)) = 0$ [24, Lemma 10.1]. Lastly, if $0 \leq \lambda_0 \leq \|C\|$ and $\lambda_1 = 0$, then from (41),

$$H(\lambda) = \lambda_0 I + C + \tilde{B}D\tilde{B}^\top \quad (44)$$

with $d_k = \frac{1}{\lambda_0/\tau + \lambda_k(A)} = \frac{1}{\lambda_k(A)} - \frac{\lambda_0/\tau}{(\lambda_0/\tau + \lambda_k(A))\lambda_k(A)} \geq \frac{1}{\lambda_k(A)} - \frac{\lambda_0/\tau}{\lambda_{\min}(A)\lambda_k(A)}$. It follows

$$\begin{aligned} H(\lambda) &\geq \lambda_0 I + C + \left(1 - \frac{\lambda_0/\tau}{\lambda_{\min}(A)}\right) BA^{-1}B^\top \\ &= \left(1 - \frac{\lambda_0/\tau}{\lambda_{\min}(A)}\right)(C + BA^{-1}B^\top) + \frac{\lambda_0/\tau}{\lambda_{\min}(A)}C + \lambda_0 I \end{aligned}$$

As $\tau > \|C\|/\lambda_{\min}(A)$, $0 \leq \lambda_0 \leq \|C\|$ we have that $0 \leq \frac{\lambda_0/\tau}{\lambda_{\min}(A)} < 1$ and that $I + \frac{1}{\tau\lambda_{\min}(A)}C$ is p.d., i.e. we find that again $H(\lambda)$ is p.d which is contradictory. In conclusion, $\lambda_0 < 0$. \square

H Proof of Theorem 3.3

As in [10, Lemma 2.7], we apply the Ky Fan inequality [39, Lemma 4.20] to analyze the symmetric part of the matrix \mathbf{M} in (39): if $\lambda_k(\mathbf{M}) = \lambda_0 + i\lambda_1$ is the k -th eigenvalue of \mathbf{M} , then its real part $\lambda_0 \leq \lambda_{\max}((\mathbf{M} + \mathbf{M}^\top)/2)$. We show that $\lambda_{\max}((\mathbf{M} + \mathbf{M}^\top)/2) < 0$. This allows one to set $\gamma^\bullet = -2 \max_k \frac{\text{Re}(\lambda_k(\mathbf{M}))}{|\lambda_k(\mathbf{M})|^2}$ as in the proof of Theorem 3.2 to conclude.

Based on the proof of [21, Proposition 26], we consider $(\bar{\mathbf{A}}, \bar{\mathbf{B}}, \bar{\mathbf{C}})$ are defined in (39))

$$\begin{aligned} \mathbf{M} &= \begin{pmatrix} 0 & \sqrt{\frac{1}{\tau}}I \\ I & 0 \end{pmatrix} \begin{pmatrix} -\bar{\mathbf{C}} & -\bar{\mathbf{B}} \\ \tau\bar{\mathbf{B}}^\top & -\tau\bar{\mathbf{A}} \end{pmatrix} \begin{pmatrix} 0 & \sqrt{\frac{1}{\tau}}I \\ I & 0 \end{pmatrix}^{-1} \\ &= \begin{pmatrix} \sqrt{\tau}\bar{\mathbf{B}}^\top & -\sqrt{\tau}\bar{\mathbf{A}} \\ -\bar{\mathbf{C}} & -\bar{\mathbf{B}} \end{pmatrix} \begin{pmatrix} 0 & I \\ \sqrt{\tau}I & 0 \end{pmatrix} = \begin{pmatrix} -\tau\bar{\mathbf{A}} & \sqrt{\tau}\bar{\mathbf{B}}^\top \\ -\sqrt{\tau}\bar{\mathbf{B}} & -\bar{\mathbf{C}} \end{pmatrix}. \end{aligned}$$

From the Ky Fan inequality, the real part of each eigenvalue λ of \mathbf{M} is upper bounded by the maximal eigenvalue of $(\mathbf{M} + \mathbf{M}^\top)/2$. We verify that indeed $\lambda_{\max}((\mathbf{M} + \mathbf{M}^\top)/2) < 0$ because $\bar{\mathbf{A}}$ and $\bar{\mathbf{C}}$ are p.d., and $\tau > 0$. Therefore, the real part of λ is strictly smaller than 0.

I Derivation of deterministic τ -SGA algorithm

The τ -SGA algorithm modifies the vector field $\xi(x, y) = (-\delta(x, y), \tau\eta(x, y))$ of τ -GDA using the anti-symmetric part of the Jacobian matrix of $\xi(x, y)$. As $\delta(x, y) = \text{grad}_x f(x, y)$ and $\eta(x, y) = \text{grad}_y f(x, y)$, the Jacobian matrix is the following linear transform on $T_x\mathcal{M}_1 \times T_y\mathcal{M}_2$ (which is a natural extension from the Euclidean case),

$$J(x, y) = \begin{pmatrix} -\tilde{\mathbf{C}}(x, y) & -\tilde{\mathbf{B}}(x, y) \\ \tau\tilde{\mathbf{B}}^\top(x, y) & -\tau\tilde{\mathbf{A}}(x, y) \end{pmatrix} = \begin{pmatrix} -\text{Hess}_x(x, y) & -\text{grad}_{yx}^2 f(x, y) \\ \tau\text{grad}_{xy}^2 f(x, y) & \tau\text{Hess}_y(x, y) \end{pmatrix}. \quad (45)$$

Here we introduce the notation $\tilde{\mathbf{A}}, \tilde{\mathbf{B}}, \tilde{\mathbf{C}}$ in (45) to simplify the equation. The τ -SGA update rule is obtained from ⁵

$$\begin{aligned} &\xi(x, y) + \mu \left(\frac{J(x, y) - J^\top(x, y)}{2} \right) \xi(x, y) \\ &= \xi(x, y) + \mu \frac{\tau + 1}{2} \begin{pmatrix} 0 & -\tilde{\mathbf{B}}(x, y) \\ \tilde{\mathbf{B}}^\top(x, y) & 0 \end{pmatrix} \xi(x, y) \\ &= \left[\begin{pmatrix} -\delta \\ \tau\eta \end{pmatrix} + \mu \frac{\tau + 1}{2} \begin{pmatrix} -\tau\tilde{\mathbf{B}}[\eta] \\ -\tilde{\mathbf{B}}^\top[\delta] \end{pmatrix} \right] (x, y). \end{aligned}$$

⁵Note that in the original SGA rule [23, Proposition 5] the transpose of $\frac{J(x, y) - J^\top(x, y)}{2}$ is considered since its definition of J has a sign difference compared to ours in (45).

We next show that the correction term, which is proportional to $(\tau\tilde{\mathbf{B}}[\eta], \tilde{\mathbf{B}}^\top[\delta])$, is orthogonal to the τ -GDA direction $(-\delta, \tau\eta)$ at each (x, y) , under the Riemannian metric on the tangent space $T_x\mathcal{M}_1 \times T_y\mathcal{M}_2$.

Proposition I.1. *For any $(x, y) \in \mathcal{M}_1 \times \mathcal{M}_2$, we have*

$$\langle \tau\tilde{\mathbf{B}}(x, y)[\eta(x, y)], \delta(x, y) \rangle_x + \langle \tilde{\mathbf{B}}^\top(x, y)[\delta(x, y)], -\tau\eta(x, y) \rangle_y = 0.$$

Proof. We follow the proof in Appendix B, by using a local coordinate chart $(O_1 \times O_2, \varphi_1 \times \varphi_2)$ around the point (x, y) rather than (x^*, y^*) . As in (17) and (18), this coordinate chart maps $\delta(x, y)$ and $\eta(x, y)$ to their local coordinates $\bar{\delta}(u_1, u_2)$ and $\bar{\eta}(u_1, u_2)$. It also induces a canonical basis $\{E_{1,i}(x)\}_{i \leq d_1}$ on $T_x\mathcal{M}_1$ and $\{E_{2,j}(y)\}_{j \leq d_2}$ on $T_y\mathcal{M}_2$. By the definition of cross-gradients,

$$\begin{aligned} \tilde{\mathbf{B}}(x, y)[\eta(x, y)] &= D_y \text{grad}_x f(x, y)[\eta(x, y)] \\ &= D_y \delta(x, y)[\eta(x, y)] \\ &= \sum_i \left(\frac{\partial \bar{\delta}_i}{\partial u_2}(u_1, u_2) \bar{\eta}(u_1, u_2) \right) E_{1,i}(x). \end{aligned}$$

Using the Riemannian metric \bar{g}_1 represented in the local coordinate as in (19), it turns out that

$$\langle \tilde{\mathbf{B}}(x, y)[\eta(x, y)], \delta(x, y) \rangle_x = \bar{\delta}(u_1, u_2)^\top \bar{g}_1(u_1) \left(\frac{\partial \bar{\delta}}{\partial u_2}(u_1, u_2) \bar{\eta}(u_1, u_2) \right). \quad (46)$$

Similarly we have

$$\langle \tilde{\mathbf{B}}^\top(x, y)[\delta(x, y)], \eta(x, y) \rangle_y = \bar{\eta}(u_1, u_2)^\top \bar{g}_2(u_2) \left(\frac{\partial \bar{\eta}}{\partial u_1}(u_1, u_2) \bar{\delta}(u_1, u_2) \right). \quad (47)$$

We conclude that (46) equals to (47) because as in (32), (33)

$$\bar{g}_1(u_1) \frac{\partial \bar{\delta}}{\partial u_2}(u_1, u_2) = \left(\bar{g}_2(u_2) \frac{\partial \bar{\eta}}{\partial u_1}(u_1, u_2) \right)^\top.$$

□

J Computational efficiency of τ -SGA

We first discuss the computation of $\tilde{\mathbf{B}}[\eta]$ and $\tilde{\mathbf{B}}^\top[\delta]$ when \mathcal{M}_1 (resp. \mathcal{M}_2) is an embedded sub-manifold of $\mathbb{R}^{d'_1}$ (resp. $\mathbb{R}^{d'_2}$). We then propose a linear-time computational procedure using auto-differentiation when \mathcal{M}_1 is Euclidean, which is applicable to Wasserstein GAN. When \mathcal{M}_2 is also Euclidean, this procedure is equivalent to the one proposed in [4].

To compute $\tilde{\mathbf{B}}[\eta]$ at (x, y) , we first fix $\eta = \eta(x, y) \in T_y\mathcal{M}_2$. From the property of embedded sub-manifolds, we use \leftrightarrow to identify a tangent vector $\delta \in T_x\mathcal{M}_1$ with a vector $\delta' = (\delta'_i)_{i \leq d'_1} \in \mathbb{R}^{d'_1}$ (resp. $\eta \in T_y\mathcal{M}_2$ with $\eta' = (\eta'_i)_{i \leq d'_2} \in \mathbb{R}^{d'_2}$).

This allows one to compute the cross-gradients in the embedded space, by

$$\tilde{\mathbf{B}}[\eta](x, y) = D_y \text{grad}_x f(x, y)[\eta] \leftrightarrow D_y \delta'(x, y)[\eta'] = \langle (\text{grad}_y \delta'_i(x, y))', \eta' \rangle_y \rangle_{i \leq d'_1} \in \mathbb{R}^{d'_1}.$$

Note that $\langle (\text{grad}_y \delta'_i(x, y))', \eta' \rangle_y$ is computed on $\mathbb{R}^{d'_2}$ with a metric induced from $T_y\mathcal{M}_2$. Assume that its computational time is $O(d'_2)$ for each i . Then it takes $O(d'_2 d'_1)$ to compute $\tilde{\mathbf{B}}[\eta](x, y)$ in the embedded space. We can obtain a similar cost for $\tilde{\mathbf{B}}^\top[\delta](x, y)$.

When $\mathcal{M}_1 = \mathbb{R}^{d_1}$, the computational complexity of $\tilde{\mathbf{B}}[\eta](x, y)$ can be significantly reduced: $\forall i \leq d_1$,

$$D_y \partial_{x_i} f(x, y)[\eta] = \partial_{x_i} \langle \text{grad}_y f(x, y), \eta \rangle_y \leftrightarrow \partial_{x_i} \langle \eta'(x, y), \eta' \rangle_y. \quad (48)$$

Importantly, one does not need to recompute $\langle \eta'(x, y), \eta' \rangle_y$ for each i . Therefore, the whole cost of $\tilde{\mathbf{B}}[\eta](x, y)$ is $O(d_1 + d'_2)$. Note that in (48), the term η' is “detached”.

For $\tilde{\mathbf{B}}^\top[\delta](x, y)$, we “detach” $\delta = \delta(x, y) \in T_x \mathcal{M}_1$ and compute

$$\tilde{\mathbf{B}}^\top[\xi_1](x, y) = \sum_{i \leq d_1} \partial_{x_i} \eta(x, y) \delta_i \quad \leftrightarrow \quad \partial_{\eta''} \left(\sum_{i \leq d_1} \partial_{x_i} \langle \eta'(x, y), \eta'' \rangle \delta_i \right) \Big|_{\eta''=0}.$$

This implies that we can first compute $\partial_{x_i} \langle \eta'(x, y), \eta'' \rangle$ for each i as in (48). We then compute its sum with δ_i which takes $O(d_1)$. Finally an extra auto-differentiation is taken with respect to η'' which costs $O(d'_2)$. The whole cost of $\tilde{\mathbf{B}}^\top[\xi_1](x, y)$ is therefore $O(d_1 + d'_2)$. Note that in this case, we use the Euclidean metric on $\mathbb{R}^{d'_2}$ to evaluate $\langle \eta'(x, y), \eta'' \rangle$ rather than the induced Riemannian metric in (48).

In the Example 2 in Figure 2 and the MNIST (digit 0) in Table 2, we find that the computational time per iteration t of τ -SGA is roughly 3-4 times that of τ -GDA.

J.1 Extension to stochastic τ -SGA

We construct stochastic τ -SGA through an unbiased estimation of terms in the update rule of deterministic τ -SGA. To achieve this, we compute $\partial_{x_i} \langle \eta'(x, y), \eta' \rangle_y$ in (48) using two mini-batches independently sampled from a training set, one to estimate $\eta'(x, y)$, the other to estimate η' . Similarly, we use the same two mini-batches to estimate $\eta'(x, y)$ and δ in $\tilde{\mathbf{B}}^\top[\xi_1](x, y)$.

K Proof of Theorem 3.4

Since f is twice continuously differentiable, we can apply Theorem 3.1 to analyze the induced dynamics $\bar{\mathbf{T}}$ (\mathbf{T} defined by (13),(14)). Following (37), we obtain

$$\bar{\mathbf{T}}(u_1, u_2) = \begin{pmatrix} \bar{\mathcal{R}}_1 \left(u_1, -\gamma \left[\bar{\delta} + \mu \frac{(\tau+1)\tau}{2} \frac{\partial \bar{\delta}}{\partial u_2} \bar{\eta} \right] (u_1, u_2) \right) \\ \bar{\mathcal{R}}_2 \left(u_2, \gamma \tau \bar{\eta}(u_1, u_2) \right) \end{pmatrix}, \quad (49)$$

Firstly, we remark that if we want to analyze the τ -SGA method beyond the asymptotic regime, one needs to consider this induced dynamics $\bar{\mathcal{R}}_2 \left(u_2, \gamma \left[\tau \bar{\eta} - \mu \frac{\tau+1}{2} \frac{\partial \bar{\eta}}{\partial u_1} \bar{\delta} \right] (u_1, u_2) \right)$ for the variable u_2 . The analysis of the spectral radius of the Jacobian matrix $\bar{\mathbf{T}}'(u_1^*, u_2^*)$ is harder as one could not easily adapt the proof of Proposition G.1 to this case. This remains an interesting open question.

From (49), we compute the Jacobian matrix $\bar{\mathbf{T}}'(u_1^*, u_2^*) = I + \gamma M$, where

$$M = \begin{pmatrix} -\frac{\partial \bar{\delta}}{\partial u_1}(u_1^*, u_2^*) & -\frac{\partial \bar{\delta}}{\partial u_2}(u_1^*, u_2^*) \\ \tau \frac{\partial \bar{\eta}}{\partial u_1}(u_1^*, u_2^*) & \tau \frac{\partial \bar{\eta}}{\partial u_2}(u_1^*, u_2^*) \end{pmatrix} - \mu \frac{(\tau+1)\tau}{2} \begin{pmatrix} [\frac{\partial \bar{\delta}}{\partial u_2} \frac{\partial \bar{\eta}}{\partial u_1}](u_1^*, u_2^*) & [\frac{\partial \bar{\delta}}{\partial u_2} \frac{\partial \bar{\eta}}{\partial u_2}](u_1^*, u_2^*) \\ 0 & 0 \end{pmatrix}$$

This can be reduced to the analysis of the eigenvalues of a similar matrix \mathbf{M} as in (39),

$$\mathbf{M} = \begin{pmatrix} -\bar{\mathbf{C}} & -\bar{\mathbf{B}} \\ \tau \bar{\mathbf{B}}^\top & -\tau \bar{\mathbf{A}} \end{pmatrix} + \mu \frac{(\tau+1)\tau}{2} \begin{pmatrix} -\bar{\mathbf{B}} \bar{\mathbf{B}}^\top & \bar{\mathbf{B}} \bar{\mathbf{A}} \\ 0 & 0 \end{pmatrix}$$

As in the proof of Theorem 3.2, we verify that $\tau > \min(\|\bar{\mathbf{C}}\|, \|\bar{\mathbf{C}} + \theta \bar{\mathbf{B}} \bar{\mathbf{B}}^\top\|) / \lambda_{\min}(\bar{\mathbf{A}})$, and $\mu = \theta \frac{2}{\tau(\tau+1)}$ with $0 \leq \theta \leq 1/\lambda_{\max}(\bar{\mathbf{A}})$. From the Proposition K.1 (see next), we conclude that the real-part of each eigenvalue of \mathbf{M} is strictly negative. Therefore as in the proof of Theorem 3.3, we can find $\gamma^\bullet > 0$ to guarantee the local convergence for $0 < \gamma < \gamma^\bullet$.

K.1 Spectral analysis of \mathbf{M}

The following proposition is adapted from Proposition G.1 to analyze the eigenvalues of \mathbf{M} .

Proposition K.1. *Let $A \in \mathbb{R}^{m \times m}$, $B \in \mathbb{R}^{n \times m}$, $C \in \mathbb{R}^{n \times n}$ such that A and $C + BA^{-1}B^\top$ are positive definite. Assume that $\tau > \min(\|C\|, \|C + \theta BB^\top\|) / \lambda_{\min}(A)$, and $\mu = \theta \frac{2}{\tau(\tau+1)}$ with $0 \leq \theta \leq 1/\lambda_{\max}(A)$, then any eigenvalue $\lambda = \lambda_0 + i\lambda_1$ (where $\lambda_0 \in \mathbb{R}, \lambda_1 \in \mathbb{R}$) of the following matrix,*

$$M = \begin{pmatrix} -C & -B \\ \tau B^\top & -\tau A \end{pmatrix} + \mu \frac{(\tau+1)\tau}{2} \begin{pmatrix} -BB^\top & BA^\top \\ 0 & 0 \end{pmatrix}$$

satisfies $\lambda_0 < 0$.

Proof. We show that $\lambda_0 \geq 0$ will lead to a contradiction, by following the proof of Proposition G.1. Assume that λ is an eigenvalue of M , i.e. $\det(\lambda I - M) = 0$. To compute $\det(\lambda I - M)$, notice that $\lambda I + \tau A$ is invertible since $\lambda_0 I + \tau A$ is positive definite (A is positive definite and $\lambda_0 \geq 0$). By the Schur complement, we have

$$\begin{aligned} \det(\lambda I - M) &= \det \begin{pmatrix} C + \theta BB^\top + \lambda I & B - \theta BA \\ -\tau B^\top & \tau A + \lambda I \end{pmatrix} \\ &= \det(\lambda I + \tau A) \det(H(\lambda)) \end{aligned} \quad (50)$$

where $H(\lambda) = \lambda I + C + \theta BB^\top + (B - \theta BA)(\lambda/\tau + A)^{-1}B^\top$. As $\lambda I + \tau A$ is invertible, $\det(\lambda I - M) = 0$ implies that $\det(H(\lambda)) = 0$.

Let the spectral decomposition of A be $U \Lambda_A U^\top$, with orthogonal $U \in \mathbb{R}^{m \times m}$ and diagonal $\Lambda_A = \text{diag}(\lambda_1(A), \dots, \lambda_m(A)) \in \mathbb{R}^{m \times m}$. Then

$$H(\lambda) = \lambda I + C + \theta BB^\top + \tilde{B} D \tilde{B}^\top,$$

with $\tilde{B} = BU$ and $D = \text{diag}(d_1, \dots, d_m)$ where

$$d_k = \frac{1 - \theta \lambda_k(A)}{\lambda/\tau + \lambda_k(A)} = (1 - \theta \lambda_k(A)) \frac{\lambda_0/\tau + \lambda_k(A) - i\lambda_1/\tau}{(\lambda_0/\tau + \lambda_k(A))^2 + (\lambda_1/\tau)^2}, \quad 1 \leq k \leq m.$$

It follows that if $\lambda_0 > \min(\|C\|, \|C + \theta BB^\top\|)$, then the real-part of $H(\lambda)$ is

$$\text{Re}(H(\lambda)) = \lambda_0 I + C + \theta BB^\top + \tilde{B} \text{Re}(D) \tilde{B}^\top \geq \lambda_0 I + C + \theta BB^\top \quad \text{p.d.} \quad (51)$$

This is contradictory to the fact that $\det(H(\lambda)) = 0$ [24, Corollary 10.2]. On the other hand, if $0 \leq \lambda_0 \leq \min(\|C\|, \|C + \theta BB^\top\|)$ and $\lambda_1 \neq 0$, then consider for $\beta \in \mathbb{R}$,

$$\begin{aligned} \text{Re}(H(\lambda)) + \frac{\tau\beta}{\lambda_1} \text{Im}(H(\lambda)) &= \lambda_0 I + C + \theta BB^\top + \tilde{B} \text{Re}(D) \tilde{B}^\top + \frac{\tau\beta}{\lambda_1} (\lambda_1 I + \tilde{B} \text{Im}(D) \tilde{B}^\top) \\ &= (\lambda_0 + \tau\beta) I + C + \theta BB^\top + \tilde{B} F \tilde{B}^\top, \end{aligned} \quad (52)$$

where $F = \text{diag}(f_1, \dots, f_m)$ with

$$f_k = (1 - \theta \lambda_k(A)) \frac{\lambda_0/\tau + \lambda_k(A) - \beta}{(\lambda_0/\tau + \lambda_k(A))^2 + (\lambda_1/\tau)^2}, \quad 1 \leq k \leq m. \quad (53)$$

Take $\beta = \lambda_{\min}(A)$, then $f_k \geq 0$ for each $k \leq m$. The condition $\tau \lambda_{\min}(A) > \min(\|C\|, \|C + \theta BB^\top\|)$ implies $(\lambda_0 + \tau\beta) I + C + \theta BB^\top$ is p.d. and together with (53), we have (52) is p.d., so it is contradictory to the fact that $\det(H(\lambda)) = 0$ [24, Lemma 10.1]. Lastly, if $0 \leq \lambda_0 \leq \min(\|C\|, \|C + \theta BB^\top\|)$ and $\lambda_1 = 0$, then from (51),

$$H(\lambda) = \lambda_0 I + C + \theta BB^\top + \tilde{B} D \tilde{B}^\top$$

with $d_k = \frac{1 - \theta \lambda_k(A)}{\lambda_0/\tau + \lambda_k(A)} = \frac{1 - \theta \lambda_k(A)}{\lambda_k(A)} - \frac{(1 - \theta \lambda_k(A)) \lambda_0/\tau}{(\lambda_0/\tau + \lambda_k(A)) \lambda_k(A)} \geq (1 - \theta \lambda_k(A)) \left(\frac{1}{\lambda_k(A)} - \frac{\lambda_0/\tau}{\lambda_{\min}(A) \lambda_k(A)} \right)$. As $\tau > \min(\|C\|, \|C + \theta BB^\top\|) / \lambda_{\min}(A)$ and $0 \leq \lambda_0 \leq \min(\|C\|, \|C + \theta BB^\top\|)$ we have $0 \leq \frac{\lambda_0/\tau}{\lambda_{\min}(A)} < 1$ and it follows

$$\begin{aligned} H(\lambda) &\geq \lambda_0 I + C + \theta BB^\top + \left(1 - \frac{\lambda_0/\tau}{\lambda_{\min}(A)} \right) BA^{-1}B^\top - \theta \left(1 - \frac{\lambda_0/\tau}{\lambda_{\min}(A)} \right) \tilde{B} \tilde{B}^\top \\ &= (1 - \lambda_0 c_0) (C + BA^{-1}B^\top) + \lambda_0 (c_0 C + c_0 \theta BB^\top + I) \\ &\geq (1 - \lambda_0 c_0) (C + BA^{-1}B^\top) \end{aligned} \quad (54)$$

where $c_0 = \frac{1}{\tau \lambda_{\min}(A)}$. The last inequity (54) is due to $\lambda_0 \geq 0$ and the condition $1 > c_0 \min(\|C\|, \|C + \theta BB^\top\|)$. They imply that $\lambda_0 (c_0 C + c_0 \theta BB^\top + I) \geq 0$. As $1 - \lambda_0 c_0 \in (0, 1]$, (54) implies that $H(\lambda)$ is p.d which is contradictory. In conclusion, $\lambda_0 < 0$. \square

L Details of numerical experiments

L.1 Choice of smooth non-linearity

We aim to build GAN models whose value function f is twice continuously differentiable, based on smooth non-linearities studied in [6]. For the discriminator of Gaussian distribution, ρ is a smooth approximation of the absolute value non-linearity of the form

$$\rho(a) = \sqrt{a^2 + \epsilon^2}, \quad \epsilon = 10^{-6}.$$

This function is twice continuously differentiable since $\rho''(a) = \frac{\epsilon^2}{2(a^2 + \epsilon^2)^{3/2}}$. Similarly, for the discriminator of MNIST digits, ρ is a smooth ReLu non-linearity,

$$\rho(a) = (a + \sqrt{a^2 + \epsilon^2})/2.$$

L.2 DCGAN generator for MNIST

We use the default DCGAN generator to model MNIST (digit 0), implemented in WGAN-GP⁶. From the 60k training samples of MNIST, we take 4932 training samples, 991 validation samples of ϕ_{data} to build the dataset MNIST (digit 0). We also make a slight modification of the generator so that the function $x \mapsto G_x(Z)$ is twice continuously differentiable at any $x \in \mathcal{M}_1$ for a given Z . For this, each ReLu non-linearity in $Z \mapsto G_x(Z)$ is replaced by the smooth ReLu ρ in Appendix L.1.

L.3 Scattering CNN discriminator for MNIST

We construct a smooth Lipschitz-continuous discriminator for MNIST digits,

$$D_y(\phi) = \langle v_y, \rho(w_y \star P(\phi) + b_y) \rangle,$$

where ρ is the smooth ReLu defined in Appendix L.1. Given ϕ , this makes the function $y \mapsto D_y(\phi)$ twice continuously differentiable at any $y \in \mathcal{M}_2$. However, the function $\phi \mapsto D_y(\phi)$ is not everywhere twice continuously differentiable due to the modulus non-linearity in the scattering transform. We therefore replace this modulus non-linearity $z \mapsto |z| = |z_{re} + iz_{im}|$ by $z \mapsto \sqrt{z_{re}^2 + z_{im}^2 + \epsilon^2}$ for each complex number input $z = z_{re} + iz_{im}$. This makes the function $\phi \mapsto D_y(\phi)$ twice continuously differentiable. As a consequence, the function $(x, y) \mapsto f(x, y)$ is also twice continuously differentiable, which is induced from the smoothness of $(x, y) \mapsto D_y(G_x(Z))$ and $y \mapsto D_y(\phi_{data})$.

Scattering transform The input ϕ of dimension $d = 784$ is represented as an image of size 28×28 . It is pre-processed by the wavelet scattering transform $P(\phi)$ to extract stable edge-like information using Morlet wavelet of different orientations and scales. We use the second-order scattering transform with four wavelet orientations (between $[0, \pi)$) and two wavelet scales. It first computes the convolution of ϕ with each wavelet filter, then a smooth modulus non-linearity is applied to each feature map. This computation is repeated one more time on each obtained feature maps and then a low-pass filter is applied to each of the channels. The obtained scattering features $P(\phi)$ is an image of size 9×9 with 25 channels ($I = 25, n = 9$).

Orthogonal CNN layer The orthogonal CNN layer is parameterized by the kernel w_y and bias b_y . The kernel w_y has 5×5 spatial size ($k = 5$). With a suitable padding and stride (two by two), we obtain an output image of size 5×5 ($N = 5$) with $J = 256$ channels. Therefore the embedding space dimension of v_y is $JN^2 = 6400$.

L.4 Stiefel manifold geometry

For the discriminators of the Gaussian distribution and MNIST (digit 0), part of the parameters in y belong to Stiefel manifolds. To choose a Riemannian metric on a Stiefel manifold (which is non-Euclidean), we use the one in [28, equation 20]. We also use the SVD projection in [28, Proposition 12] as the retraction \mathcal{R}_2 on each Stiefel manifold.

⁶<https://github.com/caogang/wgan-gp>

L.5 Initialization for local convergence

Simultaneous τ -GDA initialization for Gaussian distribution Starting from a random initialization of (x, y) , we apply the τ -GDA to build a pre-trained model. It is pre-trained with batch size 1000, learning rate $\gamma = 0.0002$ and $\tau = 100$ for $T = 50000$ iterations.

Alternating τ -GDA initialization for MNIST (digit 0) The alternating τ -GDA [40] is often used in the training of WGAN-GP [16], and it can be extended to Riemannian manifold using the retraction. Starting from a random initialization of (x, y) , we apply the alternating τ -GDA to build a pre-trained model. Each iteration amounts to perform $\tau = 5$ gradient updates of y (with learning rate 0.1) and one gradient update of x (with learning rate 0.1). It is pre-trained with batch size 128 for a total number of 10000 iterations.